Journal of Hydrology: Regional Studies 48 (2023) 101436

Contents lists available at ScienceDirect

Journal of Hydrology: Regional Studies

journal homepage: www.elsevier.com/locate/ejrh

Attributing the drivers of runoff decline in the Thaya river basin ☆

Milan Fischer [a,b,*], Petr Pavlík [c,d,**], Adam Vizina [c,d], Jana Bernsteinová [a], Juraj Parajka [e], Martha Anderson [f], Jan Řehoř [a,g], Jana Ivančicová [h], Petr Štěpánek [a,h], Jan Balek [a], Christopher Hain [i], Pavel Tachecí [j], Martin Hanel [d], Petr Lukeš [a], Monika Bláhová [a,b], Jiří Dlabal [c], Pavel Zahradníček [a,h], Petr Máca [d], Jürgen Komma [e], Nad'a Rapantová [k], Song Feng [l], Petr Janál [h], Evžen Zeman [a], Zdeněk Žalud [a,b], Günter Blöschl [e], Miroslav Trnka [a,b]

[a] Global Change Research Institute of the Czech Academy of Sciences, Bělidla 986/4a, 603 00 Brno, the Czech Republic
[b] Department of Agrosystems and Bioclimatology, Mendel University in Brno, Zemědělská 1665/1, 613 00 Brno, the Czech Republic
[c] Department of Hydrology, T. G. Masaryk Water Research Institute, Podbabská 2582/30, 160 00 Prague 6, the Czech Republic
[d] Faculty of Environmental Sciences, Czech University of Life Sciences Prague, Kamýcká 129, 165 00 Prague Suchdol, the Czech Republic
[e] Centre for Water Resource Systems, Vienna University of Technology, Karlsplatz 13/222, A-1040 Vienna, Austria
[f] Hydrology and Remote Sensing Laboratory, USDA-ARS, Beltsville, MD 20705, United States
[g] Institute of Geography, Masaryk University, Kotlářská 2, 611 37, Brno, the Czech Republic
[h] Czech Hydrometeorological Institute, Kroftova 43, 616 67, Brno, the Czech Republic
[i] Marshall Space Flight Center, Earth Science Branch, NASA, Huntsville, AL 35808, United States
[j] DHI Group, Na Vrších 1490, 100 00, Prague 10, the Czech Republic
[k] Department of Geotechnics and Underground Engineering, Faculty of Civil Engineering, VSB-Technical University of Ostrava, 17. listopadu 2172/15, 708 00, Ostrava-Poruba, the Czech Republic
[l] Department of Geosciences, University of Arkansas, Fayetteville, AR 72701, United States

ARTICLE INFO

Keywords:
Climate change
Evapotranspiration
Precipitation
Remote sensing
Runoff
Trend analysis
Water balance

ABSTRACT

Study Region: The Thaya river basin provides multiple water uses in the transboundary region of Lower Austria and Southern Moravia. Due to the low precipitation (P) to reference evapotranspiration (ET_o) ratio, the Thaya river basin is among the most sensitive to climate change in the region.

Study Focus: The main objective is to understand the changes in the water balance variables including actual evapotranspiration (ET), P and runoff (RO) and their drivers for the period 1981–2020, and 2001–2020 in the case of using remote sensing data.

New Hydrological Insights for the Region: The analyses confirm previously reported increasing trends in air temperature, ET_o, and no trends in P. ET consistently increased during spring and decreased during summer, although insignificantly. This change was associated with a significant increase of spring vegetation development followed by summer stagnation. The spring RO shows significantly decreasing trends, especially in the upland water source areas. The correlation analysis reveals a different behavior along the altitude gradient, with ET in

☆ This research was funded by the project SS01010207 of the Technology Agency of the Czech Republic, Czechia entitled "The development of tool for identification of the main water management risks at the Thaya river basin and the methodology addressing their systematic solution in the conditions of climate change" and by the project ATCZ236 of the Interreg V-A AT-CZ entitled "Climate change impacts on the water balance of the Thaya river basin". The study was also conducted with support of the project SustES – "Adaptation strategies for sustainable ecosystem services and food security under adverse environmental conditions" (CZ.02.1.01/0.0/0.0/16_019/0000797).

* Corresponding author at: Global Change Research Institute of the Czech Academy of Sciences, Bělidla 986/4a, 603 00 Brno, the Czech Republic.
** Corresponding author at: Department of Hydrology, T. G. Masaryk Water Research Institute, Podbabská 2582/30, 160 00 Prague 6, the Czech Republic.
E-mail addresses: fischer.m@czechglobe.cz (M. Fischer), petr.pavlik@vuv.cz (P. Pavlík).

https://doi.org/10.1016/j.ejrh.2023.101436
Received 30 December 2022; Received in revised form 27 May 2023; Accepted 30 May 2023
Available online 18 June 2023

the uplands generally limited by available energy whilst in the lowlands by available water in spring. In summer, however, the entire basin is often water-limited, with a more pronounced limitation in the lowlands. Complex adaptation measures reflecting the different hydroclimate relations across the altitudinal gradient are needed to sustain the water dependent sectors operating in the region facing increasing aridity.

1. Introduction

Anthropogenic global climate change is characterized by rising mean annual air temperature (T_a) and consequently an increase of potentially precipitable atmospheric water vapor (Clausius–Clapeyron equation) leading to, among others, an acceleration of the hydrological cycle (Katul et al., 2012; Vargas Godoy et al., 2021). The rate of this global hydrological cycle acceleration has been reported to vary between 2 to 7% $°C^{-1}$ (Liepert and Previdi, 2009; Wentz et al., 2007). Regionally, however, the change in climate manifests itself in numerous complex forms which can largely deviate from global values and even in the opposite direction of trends (Brázdil et al., 2021). The consequences of climate change together with impacts of land use changes on runoff (RO) in Europe have been studied extensively (Alfieri et al., 2015; Vormoor et al., 2015; Teuling et al., 2019). According to Mostowik et al. (2019), observations suggest increases of RO in northern Europe and decreases in southern Europe in the last 50 years. In Central Europe, there is a clear evidence of earlier winter floods due to a changing snow regime (Blöschl et al., 2017; Langhammer and Bernsteinová, 2020). The Czech Republic, being in the center of this region, can be regarded as an area with transitional effects of climate change on RO with site-specific phenomena. Previous studies suggest an increasing trend in mean annual, seasonal and monthly T_a (Zahradníček et al., 2021) yet hardly any trend in precipitation totals (P) at any temporal scale (Brázdil et al., 2021). Since T_a is tightly related to the atmospheric evaporative demand (Oudin et al., 2005), these two trends suggest an increasing aridity and higher likelihood of drought occurrence (Trnka et al., 2015, 2016; Hari et al., 2020). The role of the trends in T_a, P and other hydroclimate variables including vegetation, and especially their causal consequences on hydrology in the Czech Republic, has been documented only to a limited extent (Hanel et al., 2012; Blahušiaková et al., 2020). Since an increase of T_a should lead to an increase of actual evapotranspiration (ET) up to the point when it is limited by P, one might expect a notable decrease of RO and/or different storage terms of the water balance. The regional study from neighboring Austria (Duethmann and Blöschl, 2018) suggests that in the past 40 years ET has increased by ~20% while P has remained relatively constant. However, the trends in RO are often reported to be not significant (Trnka et al., 2022b) or locally even in the opposite direction (Ledvinka, 2015; Kliment et al., 2011). These trends can naturally vary over space (Ledvinka, 2015; Fiala et al., 2010), e.g. for regions where ET is prevailingly limited by energy (Kliment et al., 2011; Oulehle et al., 2021) *vs.* where it is limited by water (Trnka et al., 2022b).

The Thaya river basin, characterized by the combined influence of lower elevations and the leeward effect of the highlands from westerly directions (Řehoř et al., 2021), belongs to the basins with the lowest P to reference evapotranspiration (ET_o) ratio (Trnka et al., 2022b), making it potentially the most vulnerable larger basin to climate change in the Czech Republic. Currently, a wide spectrum of adaptation measures is being planned or implemented to mitigate the negative impacts of climate change on the landscape water balance and water resources in the Czech Republic, including the Thaya river basin (Hlásny et al., 2014; Trnka et al., 2022a,b). These adaptation measures range from purely technical (e.g. building new water reservoirs, inter-basin water transfer, irrigation) to nature-based (e.g. river renaturalization and revitalization, remediating soil proprieties, changes in crop rotations or forest species composition). In order to realistically assess their efficiency and interactions, a holistic approach is needed, allowing an accurate quantification of the basin water balance. A first step in such an analysis is to exploit the available data sets of terrestrial and remote sensing observations.

Therefore, this study aims at understanding the spatiotemporal variability and relationships in the hydroclimatic and vegetation conditions of the Thaya river basin over the last 40 years. More specifically, it examines how the climatic conditions propagate to the hydrological regime and whether the dynamics of this relationship change over time. To that end, *in situ* observations of RO and various climatological variables as well as remote sensing data describing ET, snow, and vegetation dynamics were analyzed.

We hypothesize that there exists a difference in response to rising T_a between the lower and higher elevation parts of the basin. Since ET for the lower parts is mainly limited by P, no trend in ET is expected. In contrast, the higher parts are limited rather by available energy, and hence we expect to observe an increasing trend in ET. Consequently, we expect decreasing trends of the overall RO driven by the most pronounced decreases in the higher basin parts. Besides testing these hypotheses, an analytical quantitative attribution of the expected changes in RO was conducted, aiming at disentangling the role of different climatic drivers in RO trends.

2. Materials and methods

2.1. Study area

The Thaya river basin drains a total area of 13,419 km^2 located in the southern part of the Czech Republic (83%) and the northern part of Austria (17%). The river Thaya (in the Czech language Dyje) is formed by the confluence of the Austrian (or also called German) and Moravian Thaya in Lower Austria and represents the longest tributary of the Morava river (Danube basin). The sources of the two branches are both located in the highlands at elevations of 676 m a.s.l. (AT) and 635 m a.s.l. (CZ). The main tributaries are in the Moravian part of the basin and follow mainly a NW-SE direction. The Jihlava river flows through the eponymous city

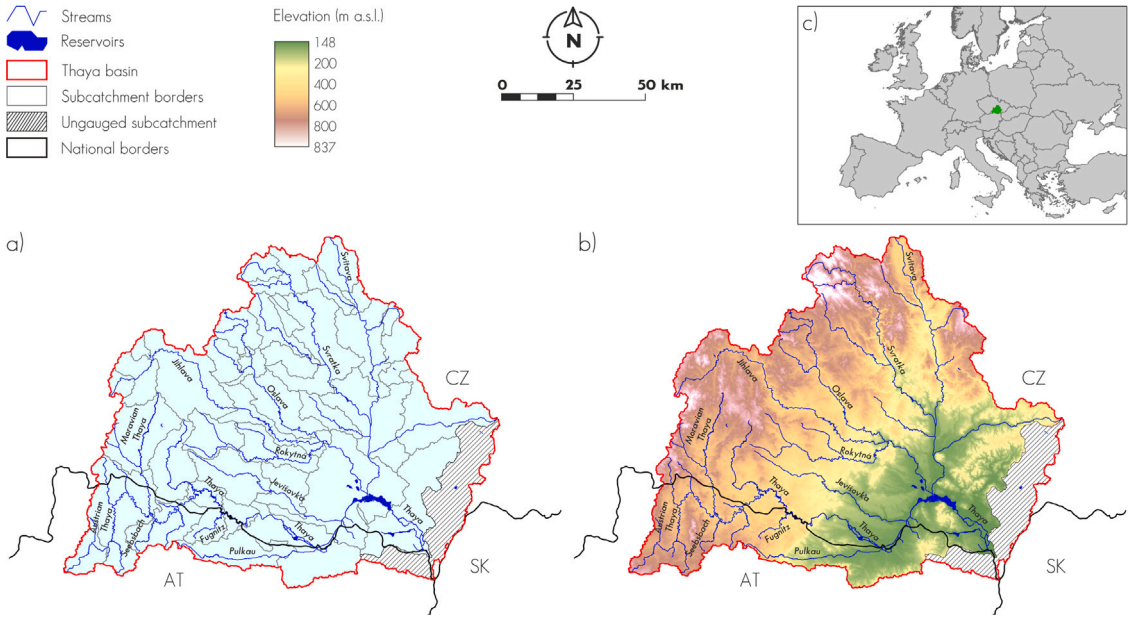

Fig. 1. (a) The Thaya river basin with 42 gauged subcatchments and river/reservoir network; (b) digital elevation model of the basin; (c) the position of the Thaya river basin within Europe.

and the Svratka together with the Svitava rivers drain Brno, the second largest city of the Czech Republic. The upper reaches of the river are formed on crystalline bedrocks while the lower parts consist of quaternary sediments. Soils follow a similar pattern and consist of predominantly cambisols in the highlands (58%) and fertile chernozems in the lower reaches (20%). The middle and lower reach of the Thaya river is characterized by anthropogenic modifications including large reservoirs constructed for water supply or irrigation purposes. The long-term annual P of the higher parts of the Thaya river basin exceeds 650 mm (Řehoř et al., 2021), and the annual RO coefficient ranges from 0.2 to 0.3 with mean annual RO of 187 mm (Trnka et al., 2022b). Nevertheless, the lowland region with lower annual P combined with high ET_o results in a significantly reduced RO coefficient (0.1–0.15) because of a mean annual RO of nearly 60 mm. The relatively limited water resources hardly satisfy the water demand of households, industry, energy and agriculture. Especially in dry years, the total water demand reaches up to 1/3 of river streamflow. As an example, during the dry period 2014–2019, drinking water supplies from the Vranov reservoir were threatened due to low water level and additional measures like usage restriction had to be imposed. The water scarcity is partly solved by water detention in 21 surface water reservoirs located at the Thaya river or tributaries.

The lowland characteristics, together with a mild and warm climate, make the agricultural landscape in the Thaya river basin fertile. Arable lands occupy 66% while forests 28% (16% coniferous, 6% mixed and 6% broadleaved) of the basin. The coniferous forests have been facing an unprecedented bark-beetle outbreak forced by high T_a and a severe drought period from 2014–2019 (Brázdil et al., 2022a). This outbreak caused a significant decay of coniferous forest stands requiring a radically increased sanitary logging which by the end of 2020 represented about 30% of the total area of coniferous stands in the basin compared to 2012.

2.2. In situ observations

The Thaya river basin excluding the confluence of the Morava river was divided into 42 topographically delineated subcatchments based on the presence of discharge gauging stations with the measurement starting in or before the year 1981. These subcatchments were considered as the main spatial units to which all other variables were aggregated. The area of 847 km^2 in the southeast near the cities Kyjov, Hodonín and Lanžhot was not represented by any discharge measurement (ungauged subcatchment) and therefore was excluded from further analyses (Fig. 1). The mean area of the subcatchments was 251 km^2, with a range from 12 km^2 to 1073 km^2.

2.2.1. Meteorological variables and snow depth

The daily meteorological data encompassed P totals, mean T_a, sums of global radiation (R_g) derived from sunshine duration, mean relative humidity (RH), and mean wind speed (u) from 50 climatological and 159 precipitation stations covering the Thaya river basin and close surroundings originating from the Czech Hydrometeorological Institute (CZ) and The Central Institute for Meteorology and Geodynamics (AT). Note that daily minimum and maximum T_a were also collected and processed, nevertheless these two variables were used only for intermediate calculations and are not part of any presented analyses. Therefore, all results

and presented analyses of T_a in this study are strictly based on mean daily T_a. The daily meteorological data were quality controlled and homogenized for the period 1981–2020 applying several methods for detecting outliers and inhomogeneities (Štěpánek et al., 2013; Brázdil et al., 2021; Zahradníček et al., 2021) and own methods for inhomogeneities corrections at daily time scale based on quantile mapping (Štěpánek et al., 2016; Squintu et al., 2020). To satisfy the requirement of the continuous time-series by further analyses, an occasionally missing data were gap-filled using a standardized procedure (Štěpánek et al., 2013).

For snow depth (SD), a process for data homogenization has not yet been standardized. Therefore, only data quality control and gap-filling (Štěpánek et al., 2013; Brázdil et al., 2021) have been performed for SD for all available stations (184) in the Thaya river basin and close surroundings.

To match the spatial coverage represented by the RO measurements, the daily data were interpolated by regression kriging into a gridded data set with a spatial resolution of 500 m, using geographical coordinates, elevation, and other terrain characteristics as kriging predictors (Štěpánek et al., 2011). The spatial resolution of 500 m was deemed to be appropriate to capture the topographical complexity while keeping a reasonable computational intensity and in addition commensurate with the resolution of other used remote sensing data. In the Thaya river basin, the average distance between two neighboring precipitation stations is less than 8 km and in the case of the variables measured at the climatological stations it is approximately 14 km. For further analyses, additional variables including actual vapor pressure (e), vapor pressure deficit (VPD), and ET_o were computed from daily inputs following the Food and Agriculture Organization of the United Nations standard methodology (Allen et al., 1998). In brief, e was computed from the saturated vapor pressure (derived as an average from daily minimum and maximum T_a using Clausius–Clapeyron equation) and RH while ET_o was computed based on the Penman-Monteith combination equation (Monteith, 1965) with strictly defined vegetation parameters (albedo, stomatal resistance, and height) and the above mentioned meteorological inputs including R_g, T_a, VPD and u (Allen et al., 1998). All meteorological data were spatially aggregated (arithmetic mean) over the 42 subcatchments.

2.2.2. Runoff

Runoff was determined from discharge measurements at the outlet of each subcatchment. The discharge data come from the network of automatic water gauging stations of the Czech Hydrometeorological Institute and the Hydrographic Service of Austria. The stations are equipped with hydrostatic pressure or ultrasonic water level sensors, from which the flow is calculated using calibrated rating curves. The daily series were aggregated to the monthly mean observed discharge (Q_o) to enable conversion into naturalized flow values (Q_n) through the methodology developed by the Ministry of Agriculture of the Czech Republic for water balance assessments at river basin scale (Tureček, 2002) working with national water usage database based on official monthly evidence. The estimation of Q_n accounts for the influence of human activities, including withdrawals, releases, and impacts of water reservoirs and reservoir management and follows as

$$Q_n = Q_o - Q_r + Q_w - \Delta Q_o, \tag{1}$$

where Q_r represents the releases to the surface water (may originate from both surface and subsurface withdrawals, including water transfer from another catchments or basins), Q_w the withdrawals from the surface and subsurface waters, and ΔQ_o the changes in observed discharge due to water manipulations, being positive if the outflow is greater than the inflow (streamflow enhancement) and negative if the outflow is smaller than the inflow (reservoir water accumulation if the sum of inflow and P exceeds the sum of outflow and open water evaporation). The naturalized streamflow data were obtained from the T. G. Masaryk Water Research Institute, representing the sole authority in the Czech Republic in charge of quality control and release of the water management data. Both Q_r and Q_w originate from the official registry of the mandatory reports, and ΔQ_o from the prescribed water reservoir ruling curves and regulation plans provided by the State Water management Enterprise in the River Morava Basin (Brno, CZ). The natural (naturalized or unimpaired) runoff depth, hereinafter just runoff (RO, mm), if not otherwise stated, was then determined by dividing Q_n by the subcatchment area, always delineated to a gauging station (we opted to use the abbreviation RO instead of Q to clearly distinguish runoff from streamflow in this text). The monthly RO time series were also used to estimate water balance evapotranspiration (ET_{WB}) as $ET_{WB} = P_c - RO$, where P_c is precipitation corrected by the snow model snowMAUS (Trnka et al., 2010) to account for the water from snowfall entering the water balance only after the snow melt.

2.3. Remote sensing data

2.3.1. Actual evapotranspiration

Actual evapotranspiration was determined by the Atmosphere-Land EXchange Inverse (ALEXI) model (Anderson et al., 1997; Hain and Anderson, 2017). ALEXI is a diagnostic model based on time-differential land surface temperature (LST) measurements and other primarily remote sensing inputs related to meteorological conditions and land cover properties. ALEXI quantifies the evaporative flux and cooling required to keep the soil and vegetation at the observed LST under the known solar radiation inputs and other meteorological conditions (Anderson et al., 2007). The core of ALEXI is a two-source energy balance (TSEB) model (Norman et al., 1995), which partitions fluxes and radiometric temperature between soil and vegetation components based on the local vegetation cover fraction apparent at the thermal sensor view angle (Anderson et al., 2007). TSEB estimates ET by partitioning the energy available at the land surface (i.e. the net radiation R_n and the soil heat flux G) into turbulent fluxes of sensible (H) and latent heat (LE) as $R_n - G = H + LE$ (all in W m^{-2}), where $LE = \lambda ET$ with λ being the latent heat of vaporization. In ALEXI, the TSEB model is coupled with a simple planetary boundary layer (PBL) model during the period of nearly linear morning T_a (as well as LST) rise (Anderson et al., 1997). Through iterative coupling, the TSEB model diagnoses the surface energy balance which in turns drives the boundary layer growth and T_a development within the PBL model, thereby constraining the gradient between LST and T_a

at the blending height (~50 m; i.e. T_a representing a mixture of landscape surfaces) required by TSEB. The morning LST rise can be directly monitored by geostationary satellites, or it can be approximated from day-night LST retrievals (Hain and Anderson, 2017). Solving this land surface-atmosphere feedback requires the model to be run at scales commensurate with surface forcing of T_a at the blending height (Mecikalski et al., 1999). For these reasons, a relatively coarse (0.05°, i.e. ~5 km) LST product aggregated from the MODIS MYD11C1 product is used for the global ALEXI version, based on day-night LST retrievals. However, for the landscape analysis, including this hydroclimatic study, finer spatial resolution is beneficial. To satisfy this need, a disaggregation (DisALEXI) and data fusion was applied (Yang et al., 2017). In DisALEXI, higher resolution remote sensing inputs of LST, leaf area index (LAI), and albedo (α) are used to spatially downscale regional ALEXI ET fluxes. In this study, MODIS inputs (e.g. MCD43A3 for α, MCD15A3H and MOD15A2H for LAI, MCD12Q1 for landcover and MOD11_L2 for LST) were used, facilitating downscaling of 5 km ALEXI ET to a spatial resolution of 500 m. The daily ET values were then spatially aggregated over the 42 subcatchments for further analyses. The subcatchment scale ET from DisALEXI was also used to quantify the surface resistance (r_s), representing a variable primarily integrating the landscape root zone water availability. The surface resistance was determined from the rewritten form of the Penman-Monteith (Monteith, 1965) equation as

$$r_s = r_a \left[\frac{\Delta}{\gamma} \frac{R_n - G}{\lambda ET} - \frac{\Delta + \gamma}{\gamma} \right] + \frac{\rho c_p}{\gamma} \frac{VPD}{\lambda ET}, \quad (2)$$

where r_a is the aerodynamic resistance, Δ is the slope of saturation vapor pressure curve with respect to T_a, γ is the psychrometric constant, ρ is the air density, and c_p is the specific heat of moist air.

2.3.2. Albedo, leaf area index, and normalized difference vegetation index

The MODIS albedo product MCD43A3, covering the period data 2001–2020, was used as an input for DisALEXI and as one of the variables within the time-series analysis. The LAI (m^2 m^{-2}) data covering the period 2001–2020 were obtained from the combination of 4-day and 8-day MODIS LAI composite products (MCD15A3H and MOD15A2H). The reason for combining these two LAI products is because the MCD15A3H is preferred for DisALEXI, due to its higher frequency of images, but available only since summer 2002. Therefore, MOD15A2H was used for the years 2001 and 2002. To provide temporally continuous time-series and to minimize the noise in the original data, a FlexFit (Gao et al., 2020) moving window filter approach using the polynomial fitting from nearby dates was used. These data were used as an input for DisALEXI as well as for LAI time-series analyses. Besides MODIS LAI, a product from the Copernicus Global Land Service (CGLS) project providing LAI based on SPOT-VGT (from 2001 to 2014) and PROBA-V (from 2014 to 2020) satellite data (1 km resolution) was tested. Normalized difference vegetation index (NDVI) time-series covering the period 1981–2020 were prepared from combination of Advanced Very High Resolution Radiometer (AVHRR) data (1 km resolution) and the MODIS NDVI product MOD13A1 (250 m resolution). For the purpose of the time series analyses, all mentioned variables were spatially aggregated (arithmetic mean) into 42 subcatchments.

2.3.3. Snow cover

Snow cover fraction (SCF) was estimated from the MODIS–Terra satellite dataset (Hall and Riggs., 2021), using daily images with a spatial resolution of 500 m (MOD10A1) for the period 2001–2020. Snow-covered pixels were identified by using the Normalized Difference Snow Index (Hall and Riggs, 2011) and classified as snow if the index is larger than 0.4 (Tong et al., 2020). The mean monthly, seasonal, or annual snow cover area of each subcatchment was estimated from the days when cloud coverage was smaller than 60%. The snow cover fraction for those days was estimated as a ratio between the frequency of pixels classified as snow and the sum of pixel frequencies classified as snow and land.

2.4. Data analyses

2.4.1. Temporal trends and correlation analyses

To analyze the possible trends in time-series of individual variables, the non-parametric Theil–Sen regression was applied (Theil, 1950; Sen, 1968). The related statistical significance of the trends was evaluated using the non-parametric Mann–Kendall test (Mann, 1945; Kendall and Gibbons, 1990). These tests were applied on temporally aggregated data covering either the entire year, growing season (April to September), or four individual seasons: December–February (DJF), March–May (MAM), June–August (JJA), and September–November (SON). To quantify a correlation between all variables, a Kendall rank correlation (Kendall, 1938) was applied. For specific analysis where variables needed to be scaled to a similar magnitude, a z-score transformation was applied, i.e. deviation from the mean normalized by standard deviation. In order to show the long-term variation, the time series were smoothed with a low-pass Gaussian filter applied in the frequency domain (fast Fourier transform). While the trend analyses were conducted for both 40 and 20-year series, the results from the 20-year series were interpreted with high caution, due to their borderline length for a trend analysis. The main justification for performing the trend analysis over the 20-year series is to utilize the remote sensing methods as a unique opportunity to gain more insights into hydroclimate processes and their temporal changes.

2.4.2. Attribution analysis

Over a sufficiently long period of time, such that the storage fluctuations are negligible, the overall water balance can be simplified to $RO \approx P - ET$ (Katul et al., 2012). As a consequence, the mass conservation law provides that changes in RO can be attributed directly to changes in P and ET as

$$\delta RO \approx \delta P - \delta ET. \quad (3)$$

Table 1
Sens's slopes and Mann–Kendall significance for the trend analysis of different variables for the 1981–2020 period at different aggregation time scales: annual (AN), growing season (GS), i.e. April to September, and seasons, i.e. 3-months period labeled by the combination of the first letter of each month. The listed variables include water vapor pressure (e), reference evapotranspiration (ET_o), water balance based actual evapotranspiration (ET_{WB}), normalized difference vegetation index based on Advanced Very High Resolution Radiometer ($NDVI_{AVHRR}$), precipitation (P), climatic water balance ($P-ET_o$), global radiation (R_g), relative humidity (RH), runoff (RO), snow depth (SD), air temperature (T_a), wind speed (u), and vapor pressure deficit (VPD). The trends are expressed as change per 10 years. All the water fluxes are expressed in mm per time and their temporal aggregation is a sum per period. Therefore, for example, for AN the units of the P trend are mm yr^{-1} $decade^{-1}$, while for GS mm (6 months)$^{-1}$ $decade^{-1}$, and for DJF mm (3 months)$^{-1}$ $decade^{-1}$.

Variable	Period					
	AN	GS	DJF	MAM	JJA	SON
e (kPa)	+0.028***	+0.032***	+0.019*	+0.017	+0.046***	+0.034***
ET_o (mm)	+13.37*	+12.70*	+0.51	+5.24	+8.46*	−1.01
ET_{WB} (mm)	+13.38	+7.39	+0.75	−0.57	+4.02	+8.19
$NDVI_{AVHRR}$	+0.042***	+0.032***	+0.054***	+0.054***	+0.022***	+0.041***
P (mm)	+7.01	+3.57	−3.18	−2.56	+4.29	+7.64
$P-ET_o$ (mm)	−6.45	−13.54	−3.11	−8.41	−3.63	+8.75
R_g (MJ m^{-2})	+36.62	+34.15	−0.57	+21.61	+10.71	−1.07
RH (%)	−0.16	−0.68	+0.31	−0.74	−0.50	+0.63
RO (mm)	−5.65	−2.93	−1.07	−5.51**	−0.30	−0.29
SD (cm)	−0.25*	–	−0.75*	−0.05	–	−0.01
T_a (°C)	+0.51***	+0.49***	+0.49*	+0.42*	+0.69***	+0.41**
u (m s^{-1})	−0.13***	−0.12***	−0.12***	−0.12***	−0.11***	−0.13***
VPD (kPa)	+0.015*	+0.031**	+0.002	+0.020*	+0.041**	−0.002

*Denotes the statistical significance of trends with $0.01 > p \leq 0.05$.
**Denotes the statistical significance of trends with $0.001 > p \leq 0.01$.
***Denotes the statistical significance of trends with $p \leq 0.001$.

The changes in ET are more complex and can be decomposed by applying partial derivatives of the Penman-Monteith model. An approximation using a first-order Taylor series expansion can be written as (Beven, 1979)

$$\delta ET \approx \frac{\partial ET}{\partial T_a}\delta T_a + \frac{\partial ET}{\partial (R_n - G)}\delta(R_n - G) + \frac{\partial ET}{\partial RH}\delta RH + \frac{\partial ET}{\partial u}\delta u + \frac{\partial ET}{\partial r_s}\delta r_s\,, \tag{4}$$

where the terms on the right-hand side represent contributions of T_a, available energy $R_n - G$, RH, u and r_s, respectively. The partial derivatives of the Penman-Monteith can also be solved using second-order (or higher order) Taylor series expansion (Feng and Fu, 2013; Chen et al., 2020). However, our results did not provide a clear evidence of additional benefit of the higher order expansion and hence we used the simpler and more straightforward (e.g. not requiring the interpretation of complex interactive terms) expression described in Eq. (4). The attribution analysis in this study was based on the application of the above mentioned expressions (Eqs. (3) and (4)), with the changes determined as the Sen's slope per decade (i.e. 10 years).

2.4.3. Budyko framework

The Budyko (1974) framework was used to analyze the long-term state and potential shifts in the evaporative index ET/P along the aridity index ET_o/P due to the changes in climate but also possibly other factors like vegetation cover (Li et al., 2013). The one-parameter function (Choudhúry, 1999)

$$\frac{ET}{P} = \frac{1}{\left[1 + (P/ET_o)^n\right]^{1/n}}\,, \tag{5}$$

with the parameter n describing the shape of the Budyko curve was fitted to the observed data. The higher values of the parameter n suggest a steeper shape of the Budyko curve and P partitioning favoring more ET than RO. The parameter n is empirically related (positive correlation) with vegetation cover, NDVI or LAI (Li et al., 2013) and thus allows to attribute the changes in P partitioning within the Budyko space to changes in climate and vegetation separately.

3. Results

3.1. Temporal trends

3.1.1. Trends over the period 1981–2020

The time series analysis of climate variables over the entire basin at the annual time scale over the period 1981–2020 revealed statistically significant increasing trends in e, ET_o, T_a and VPD, as well as statistically significant decreasing trends in SD and u (Table 1). Highly significant was also an increasing trend in NDVI (Table 1). Although statistically not significant, increasing trends in annual P, decreasing climatic water balance $P - ET_o$ and decreasing RO are also relevant for this study. Trends with similar significance and direction, yet different slopes, were detected for the above-mentioned variables also during the growing season period (April to September). When analyzing the trends for different parts of the season, consistently positive and significant

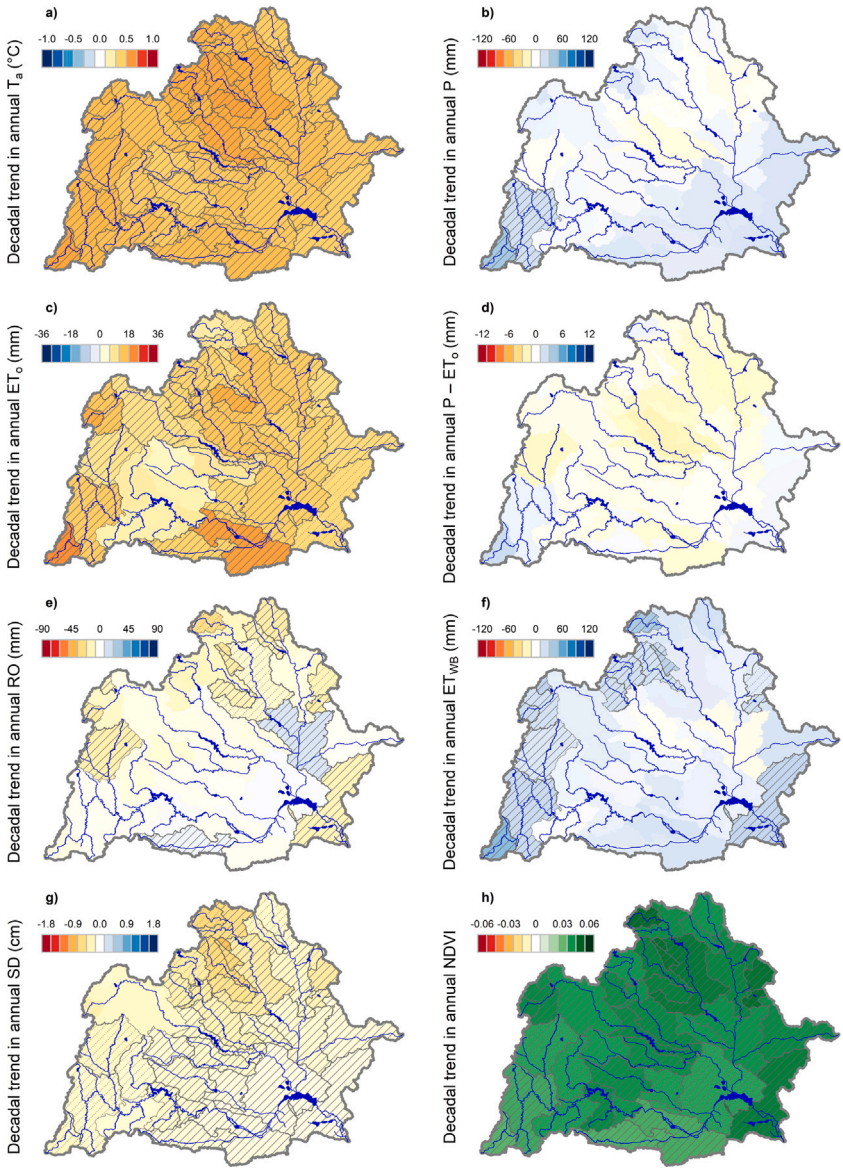

Fig. 2. Sens's slopes (color scale) and Mann–Kendall significance (crosshatch lines if $p \leq 0.05$ and dotted lines if $0.05 > p \leq 0.1$) from the trend analyses over the 42 subcatchments of the Thaya river basin for the period 1981–2020 at the annual time scale. The analyzed variables include air temperature (T_a), precipitation (P), reference evapotranspiration (ET_o), climatic water balance ($P - ET_o$), runoff (RO), water balance based actual evapotranspiration (ET_{WB}), snow depth (SD) and normalized difference vegetation index (NDVI) based on Advanced Very High Resolution Radiometer (AVHRR). Note that the ranges differ for different variables and are set to accommodate also the trends for the period 2001–2020 (Fig. 5) for easier visual comparison. Also note that the color scale is designed in a way that the red color is associated with increasing aridity or potential drought stress and therefore it is opposite in the panels a and c compared to the remaining panels. (For interpretation of the references to color in this figure legend, the reader is referred to the web version of this article.)

trends were observed in the case of T_a and NDVI, and consistently negative and significant trends in the case of u. The steepest decrease in RO was detected in spring when the trends were also significant. For the remaining parts of the year, the trends were also negative, yet not statistically significant. Despite the significant increases in T_a, ET_o increased primarily during the summer months, accompanied by the steepest and most significant increase of VPD. The contribution of trends in individual components of evaporative demand and ET are elaborated in Section 3.3.

The spatial patterns of the subset of variables listed in Table 1 were highly consistent for T_a, ET_o and NDVI, showing overall positive and significant trends over most of the entire basin (Fig. 2). Consistently negative trends were observed only for SD. In some areas (primarily those at higher elevations), statistically significantly decreasing trends were also observed for RO. Some areas also showed statistically significantly increasing trends in ET_{WB}. Precipitation and $P - ET_o$ showed no statically significant trends except in two neighboring subcatchments in the southwest of the basin in the case of P.

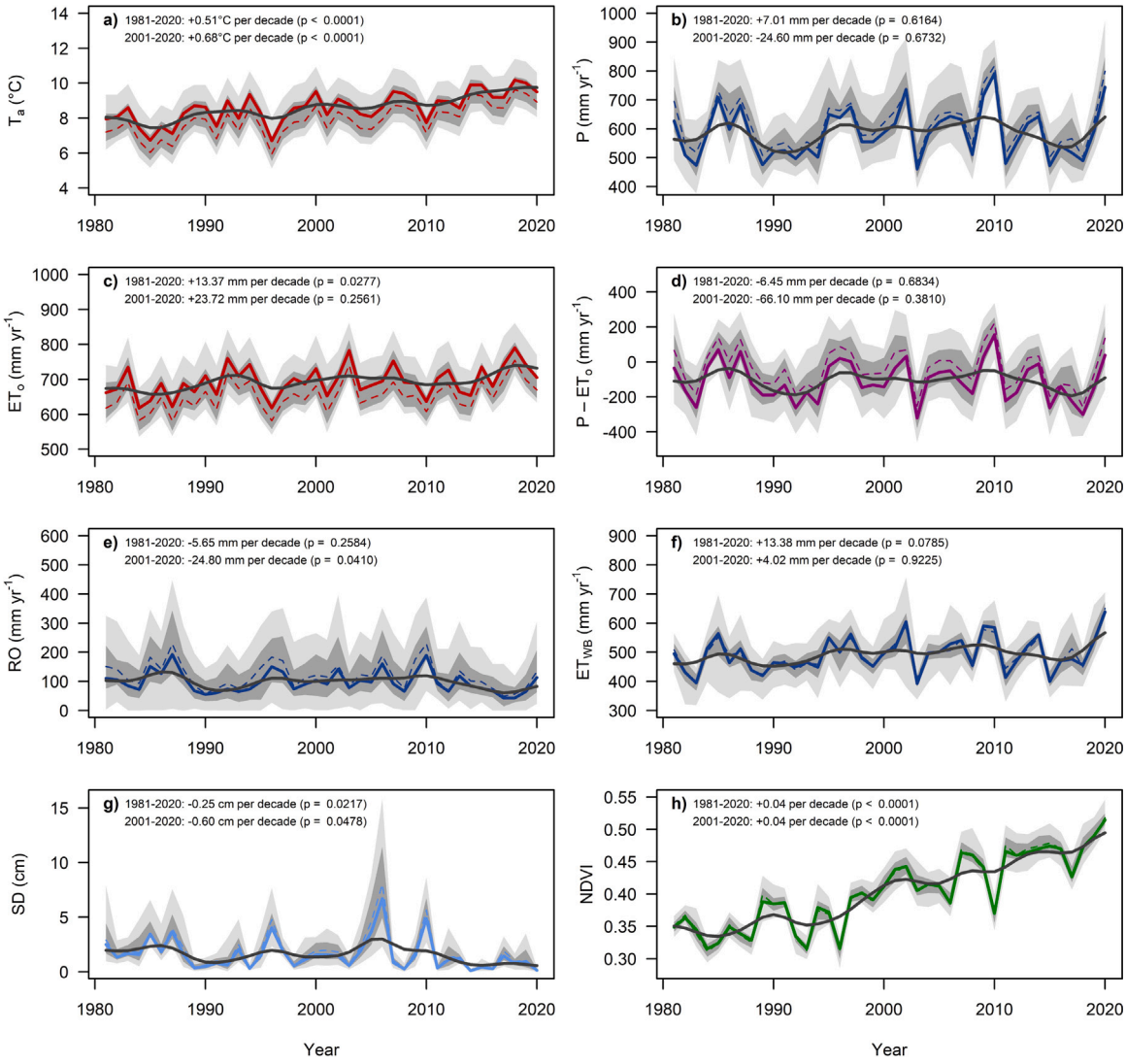

Fig. 3. Temporal trends in (a) air temperature (T_a), (b) precipitation (P), (c) reference evapotranspiration (ET_o), (d) climatic water balance ($P - ET_o$), (e) runoff (RO), water balance based actual evapotranspiration (ET_{WB}), (f) snow depth (SD), and (g) normalized difference vegetation index (NDVI) based on Advanced Very High Resolution Radiometer (AVHRR). The solid colored line depicts the given variable over the entire basin, the dashed line represents the median of all subcatchments, and the gray bands the 5, 25, 75 and 95 percentiles of all subcatchments. The solid dark gray line depicts the time series smoothed with a 10-year Gaussian filter. P-values and Sen's slopes per decade are provided. (For interpretation of the references to color in this figure legend, the reader is referred to the web version of this article.)

The most significant trend (Table 1 and Fig. 3) and the most consistent low-frequency temporal variation was a characteristic of T_a which, when smoothed by a 10-year Gaussian filter, showed a predominantly increasing tendency (Fig. 3). A similar situation was also identified for NDVI, while ET_o showed a few more pronounced decreasing periods. Low P and $P - ET_o$ were observed in 1983, at the end of the 80 s and in the first half of the 90 s, and in the years 2003, 2008, 2011, 2015 and 2017. The period 2015–2019 was identified as the period with the most negative $P - ET_o$ and was also characterized by a decrease in RO. In contrast, high P and high RO were observed in 1985, 1987, 1997, 2002, 2010 and 2020. The highest SD was recorded during the winter of 2005/2006, followed by high RO after the snow melt.

An additional inspection of longer term temporal trends using a 20-year running window (Fig. 4) revealed that at the annual and growing season time scale, only T_a and NDVI showed consistently increasing trends. The remaining variables showed periods with increasing as well as decreasing trends. An obvious switch from positive to negative trends around the window ending in 2013 (i.e. the period 1994–2013) was observed for ET_{WB}, P, $P - ET_o$ and RO. A similar switch in the trend sign also occurred in the case of SD a few years earlier. In terms of individual seasons, noteworthy is the declining tendency in the positive trend of NDVI in summer, when in 2020 (i.e. for the period 2001–2020) the first negative trend was observed. The period 2001–2020, for which more satellite data sets are available, is discussed in more detail in the next section.

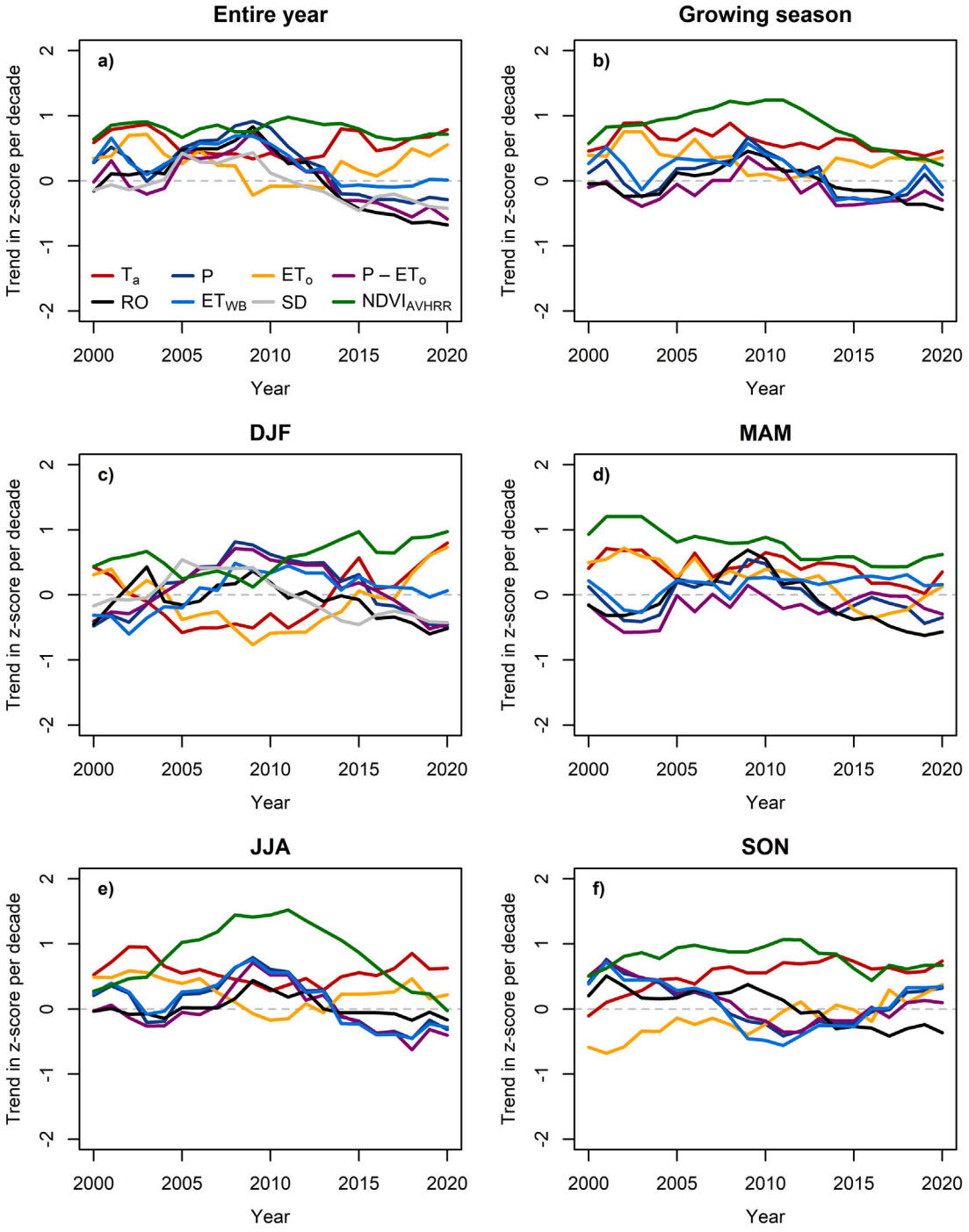

Fig. 4. Running trends (20-year long window aligned to the right) of different variables (z-score transformation) including air temperature (T_a), precipitation (P), reference evapotranspiration (ET_o), climatic water balance ($P - ET_o$), runoff (RO), water balance based actual evapotranspiration (ET_{WB}), snow depth (SD), and normalized difference vegetation index based on Advanced Very High Resolution Radiometer ($NDVI_{AVHRR}$). The growing season represents the period from April to September and the seasons are represented by 3-month periods labeled by the combination of the first letter of each month. The presented years depict the end of the 20-year long running window within the period 1981–2020.

Table 2
Sens's slopes and Mann–Kendall significance for the trend analysis of climatological variables and runoff for the period 2001–2020 at different aggregation time scales: annual (AN), growing season (GS), i.e. April to September, and seasons, i.e. 3-months period labeled by the combination of the first letter of each month. The listed variables include albedo based on Moderate Resolution Imaging Spectroradiometer (α_{MODIS}), water vapor pressure (e), reference evapotranspiration (ET_o), land surface temperature based actual evapotranspiration (ET_{LST}), water balance based actual evapotranspiration (ET_{WB}), leaf area index based on Copernicus Global Land Service (LAI_{CGLS}), LAI based on MODIS (LAI_{MODIS}), normalized difference vegetation index based on Advanced Very High Resolution Radiometer ($NDVI_{AVHRR}$), NDVI based on MODIS ($NDVI_{MODIS}$), precipitation (P), climatic water balance ($P - ET_o$), ET_{LST} based surface resistance (r_s), global radiation (R_g), relative humidity (RH), runoff (RO), snow cover fraction based on MODIS (SCF_{MODIS}), snow depth (SD), air temperature (T_a), wind speed (u), and vapor pressure deficit (VPD). The trends are expressed as change per 10 years.

Variable	Period					
	AN	GS	DJF	MAM	JJA	SON
α_{MODIS}	−0.016	+0.004***	−0.061	−0.002	+0.003*	+0.003
e (kPa)	+0.029*	+0.027	+0.045	−0.002	+0.024	+0.047*
ET_{LST} (mm)	−1.45	−3.01	+1.88	+5.16	−6.60	−3.79
ET_o (mm)	+23.72	+13.82	+3.80	+2.52	+5.84	+3.87
ET_{WB} (mm)	+0.69	−5.68	+1.55	+3.72	−13.32	+12.11
LAI_{CGLS} (m^2 m^{-2})	+0.072	+0.009	+0.110**	+0.154	−0.138	+0.078
LAI_{MODIS} (m^2 m^{-2})	+0.192***	+0.089*	+0.337***	+0.214*	+0.003	+0.233***
$NDVI_{AVHRR}$	+0.040***	+0.011	+0.082**	+0.049*	−0.001	+0.040
$NDVI_{MODIS}$	+0.054**	+0.014	+0.109**	+0.058*	−0.002	+0.037**
P (mm)	−24.60	−15.61	−12.53	−10.67	−18.40	+12.92
$P - ET_o$ (mm)	−66.10	−30.35	−12.22	−13.40	−30.86	+4.60
r_s (s m^{-1})	+15.12	+16.49	+7.88	+6.93	+20.49	+31.38
R_g (MJ m^{-2})	+43.65	+18.00	−4.78	−14.59	+15.75	+7.51
RH (%)	−1.00	−1.92	+0.02	−2.45	−1.27	−0.28
RO (mm)	−24.80*	−10.18	−5.35	−11.75*	−2.09	−3.25
SCF_{MODIS}	−0.052*	–	−0.164*	−0.003	–	−0.005
SD (cm)	−0.60*	–	−1.85*	−0.15	–	−0.06
T_a (°C)	+0.68**	+0.41	+1.31*	+0.38	+0.74	+0.71*
u (m s^{-1})	−0.13**	−0.21***	−0.02	−0.07	−0.22**	−0.16
VPD (kPa)	+0.032	+0.044	+0.012	+0.030	+0.075	+0.018

*Denotes the statistical significance of trends with $0.01 > p \leq 0.05$.
**Denotes the statistical significance of trends with $0.001 > p \leq 0.01$.
***Denotes the statistical significance of trends with $p \leq 0.001$.

3.1.2. The trends over the period 2001–2020

Compared to 1981–2020, the period 2001–2020 was generally characterized by steeper trends for all of the investigated variables except for NDVI, yet more often insignificant due the shorter length of the analyzed period (Table 2). For instance, although T_a showed positive trends across all the investigated time blocks, these trends were significant only at the annual time scale and during the fall and winter months. Similar to the 1981–2020 interval, NDVI showed increasing trends for all the seasons, yet these trends were significant only at the annual time scale and for the early and late seasons (growing season NDVI did not change significantly). LAI similarly increased during these seasons, although MODIS LAI showed a higher rate of increase than CGLS. The small and in some cases negative trends in LAI and NDVI during the summer periods may indicate vegetation stress due to water limitations. Water limitations are also supported by ET_{LST} and ET_{WB} which both showed negative anomalies with the most pronounced declines in summer during the last decade (Table 2, Fig. 6). Precipitation and $P - ET_o$ showed both insignificantly decreasing trends during all investigated time blocks except for fall when a small positive insignificant trend was detected. Similarly to 1981–2020, SD and for 2001–2020 available SCF showed statistically significantly decreasing trends. Importantly, for the period 2001–2020, RO showed statistically significant decreasing trends at the annual time scale with the steepest changes occurring again in the spring months.

The steeper trends for 2001–2020 *vs*. 1981–2020 are very evident in comparing the spatial trend maps (*cfr*. Figs. 2 and 5). Also noteworthy is the change of sign of trend in P between these two investigated periods, from positive to negative. In general, all the investigated variables suggest a shift of the entire basin towards more arid conditions characterized by more frequent drought stress. This shift appears to be more pronounced for the upper subcatchments of the basin.

The temporal variation of additional MODIS-based variables (SCF, NDVI and LAI) available for 2001–2020 (Fig. 6) are in line with those presented for 1981–2020 (SD and $NDVI_{AVHRR}$). Trends in α also depend on the land-cover and studied season. Overall, a more pronounced decreasing trend of α was observed for the urban, agriculture and grassland categories and the least for the forest categories. In terms of season, the declining trend was most pronounced for the DJF period due to the presence of snow. Albedo at the annual time scale is also strongly affected by winter snow cover and hence its peaks coincide with the peaks in SCF. Notably, MODIS-based ET_{LST} and the derived r_s indicate the dry years of 2003, 2007, 2012, 2015, 2017, and 2018 more clearly than the vegetation indices NDVI and LAI. This is partly due to increases in the vegetation indices during the off-season period. However, it should be stressed that detection of drought based on annual data can smear our short-term droughts. This is e.g. the case in 2018 which showed strongly positive anomalies in NDVI, LAI and ET during the spring which compensate negative summertime anomalies due to drought.

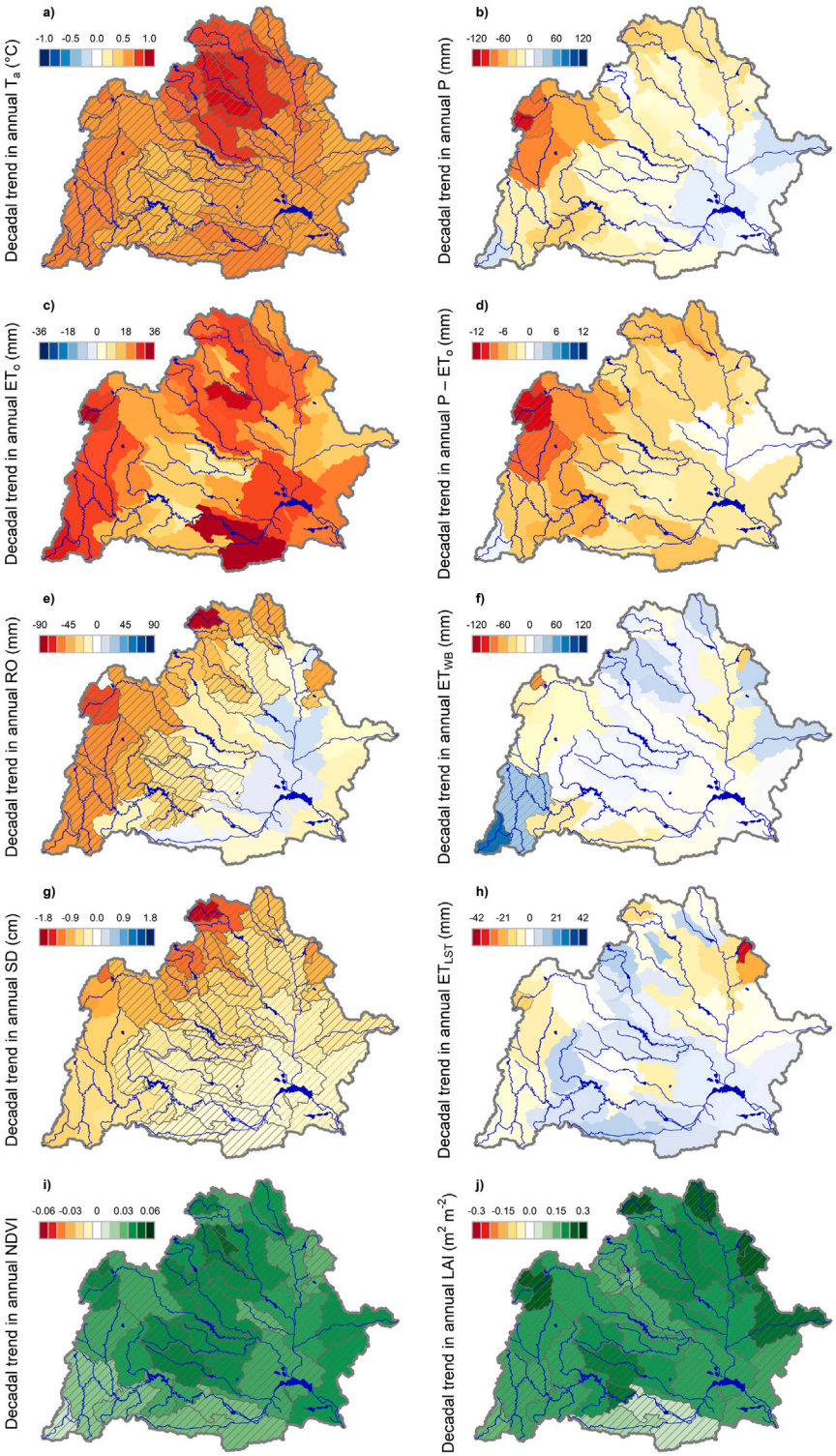

Fig. 5. Sens's slopes (color scale) and Mann–Kendall significance (crosshatch lines if $p \leq 0.05$ and dotted lines if $0.05 > p \leq 0.1$) from the trend analysis over the 42 subcatchments of the Thaya river basin for the period 2001–2020 at the annual time scale. The analyzed variables include air temperature (T_a), precipitation (P), reference evapotranspiration (ET_o), climatic water balance ($P - ET_o$), runoff (RO), water balance based actual evapotranspiration (ET_{WB}), snow depth (SD), land surface temperature based actual evapotranspiration (ET_{LST}), normalized difference vegetation index (NDVI) and leaf area index (LAI). The last three mentioned variables are based on Moderate Resolution Imaging Spectroradiometer (MODIS). Note that the ranges differ for different variables and that the color scales differ as well in a way that the red color is associated with increasing aridity or potential drought stress. (For interpretation of the references to color in this figure legend, the reader is referred to the web version of this article.)

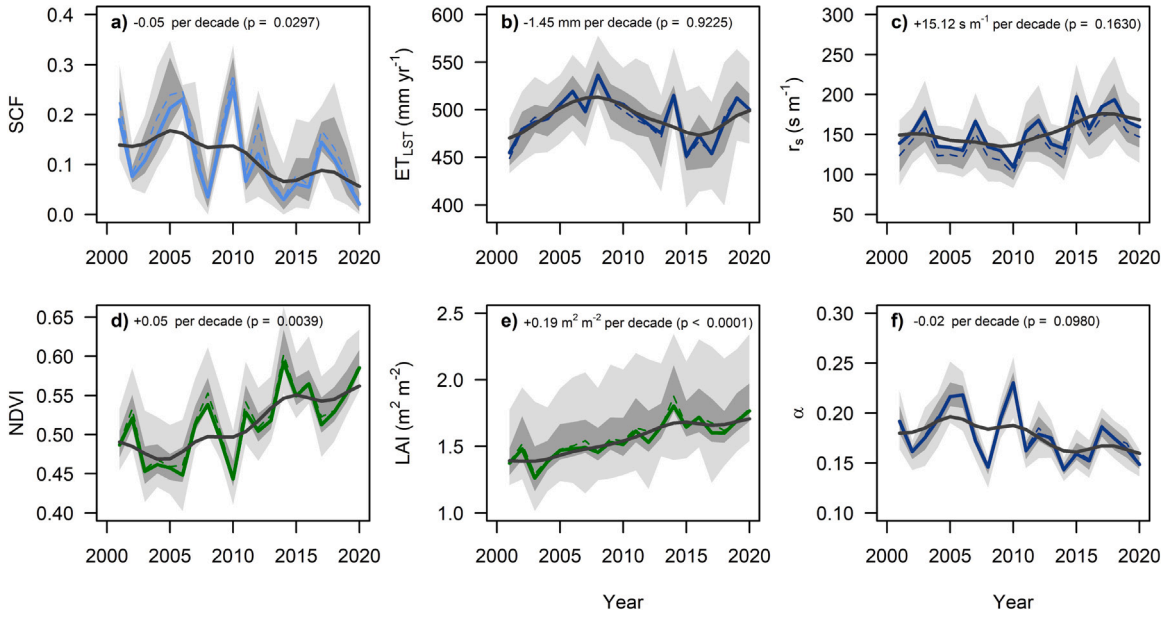

Fig. 6. Temporal trends in Moderate Resolution Imaging Spectroradiometer (MODIS) based variables including (a) snow cover fraction (SCF), (b) land surface temperature based actual evapotranspiration (ET_{LST}), (c) surface resistance (r_s), (d) normalized difference vegetation index (NDVI), (e) leaf area index (LAI), and (f) surface albedo (α). The solid colored line depicts the given variable over the entire basin, the dashed line is representing the median of all subcatchments, and the gray belts the 5, 25, 75 and 95 percentiles of all subcatchments. The solid dark gray line depicts the smoothed time series with 10-years Gaussian filter. P-values and Sen's slopes per decade are also provided. (For interpretation of the references to color in this figure legend, the reader is referred to the web version of this article.)

3.2. Correlation analysis

A pairwise correlation for variables potentially related to RO was conducted for annual and sub-annual time scales for both periods 1981–2020 as well as 2001–2020. For the period 1981–2020 (Fig. 7), RO positively correlates with P, $P - ET_o$, ET_{WB} and SD while negatively with ET_o and T_a. All the correlations are significant. The only insignificant (positive) correlation of RO is with NDVI. Similar relationships were found for the growing season. The correlation between RO and NDVI became significant for spring (negative) and summer (positive) months. Such behavior indicates that RO is reduced if spring is warmer and vegetation more developed, while during the summer, both RO and vegetation growth (NDVI) are limited by P. The stronger dependence of RO on P during the summer is also evident from the strength of the correlation between these two variables.

Similar relationships can be observed in the period 2001–2020 (Fig. 8) although, due to the shorter period of the correlation analysis, they are more frequently insignificant. The surface resistance, representing the level of landscape water stress, negatively correlated with series of variables including P, RO and ET. In contrast, it showed highly positive correlation with ET_o, meaning that higher ET_o itself is often associated with higher landscape water deficit. The impacts of water stress on vegetation are also reflected by the negative correlation of r_s with LAI and NDVI in summer. For this period one can observe the above-mentioned switch in the relationship between RO and the vegetation development (NDVI and LAI) during spring and summer even more clearly, likely due to the generally drier character of this period. In contrast to ET_{WB}, there is an insignificant relationship between ET_{LST} and RO. Nevertheless, it is worth mentioning that this relationship is negative during spring while positive during the summer months. Further insights to these relationships are provided by exploring the spatial patterns of the correlations between RO and ET_{LST} (Fig. 9a). This analysis indicates that the higher elevation subcatchments in the southeast often show a significantly negative correlation between RO and ET_{LST} during the spring months. In contrast, during the summer months the relationship becomes positive and is significant in the lower elevation areas. Note that some of the subcatchments do not obey this pattern as result of water reservoirs that do not strictly follow the water management plan (personal communication with the State enterprise Morava River Basin, Brno, CZ), leading to additional challenges to provide truly unimpaired RO time series (Eq. (1)).

For completeness, the analyses of the correlation between ET_{LST} with P (Fig. 9b), T_a (Fig. 9c), and ET_o (Fig. 9d) are provided. This analysis explains why no correlations are found when the basin is treated as a whole. In spring, there is a distinct boundary between subcatchments where ET_{LST} and P are negatively correlated in higher elevation areas and positively correlated in lower elevation areas. In summer, the entire basin shows a positive relationship between ET_{LST} and P, but only in the lower elevation areas is this correlation significant. This suggests that, during the summer, ET_{LST} at the entire basin scale is limited by P and that this limitation is stronger in the lower elevation areas. In these areas ET is limited by P also during the spring, while in the higher elevation areas ET is limited by T_a (Fig. 9a), or more generally by the available energy. The boundary delimiting this contrasting behavior can be approximated by the contour line at 450 m a.s.l.

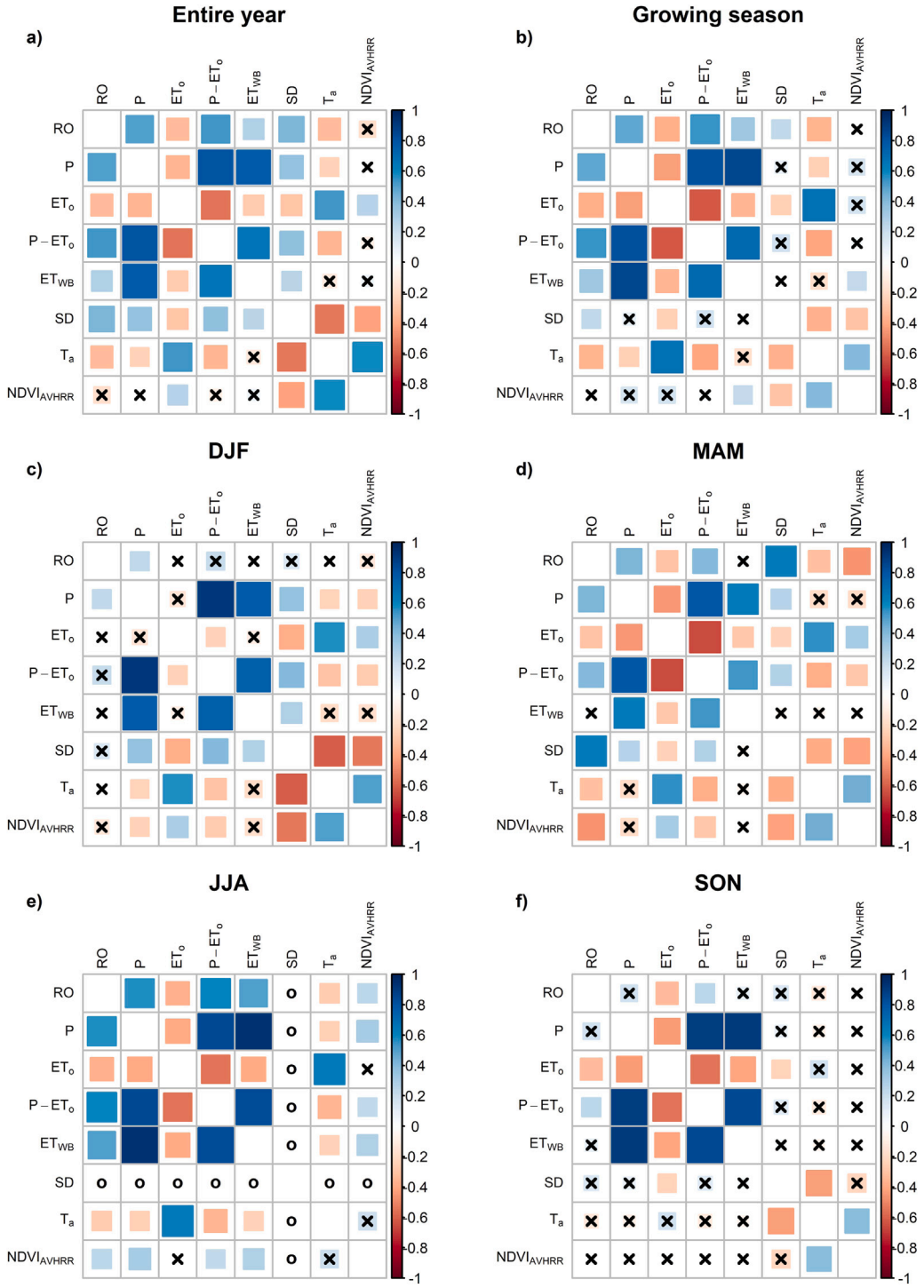

Fig. 7. Kendall rank correlation matrix of different variables for 1981–2020. The analyzed variables include runoff (RO), precipitation (P), reference evapotranspiration (ET_o), climatic water balance ($P - ET_o$), water balance based actual evapotranspiration (ET_{WB}), snow depth (SD), air temperature (T_a), and normalized difference vegetation index based on Advanced Very High Resolution Radiometer ($NDVI_{AVHRR}$). Growing season represents the period from April to September and the seasons are represented by 3-months period labeled by the combination of the first letter of each month. The strength of the correlation is visualized by intensity of the color, where red depicts a negative whilst blue a positive correlation. The crosses indicate insignificant correlation ($p > 0.05$) and the circles indicate no data during the period. (For interpretation of the references to color in this figure legend, the reader is referred to the web version of this article.)

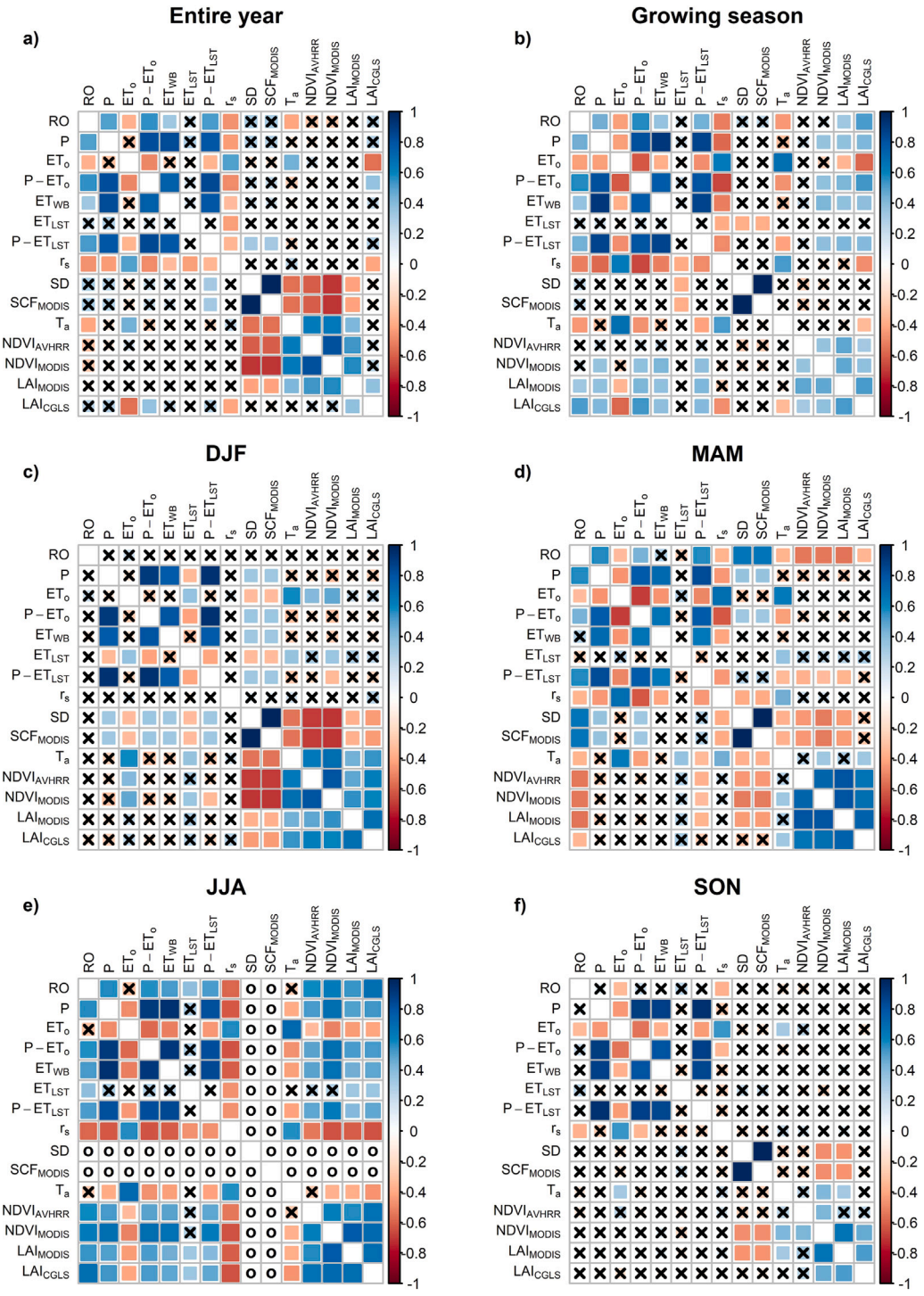

Fig. 8. Kendall rank correlation matrix of different variables for 2001–2020. The analyzed variables include runoff (RO), precipitation (P), reference evapotranspiration (ET_o), climatic water balance ($P - ET_o$), water balance based actual evapotranspiration (ET_{WB}), land surface temperature based actual evapotranspiration (ET_{LST}), approximation of RO given as the difference of P and ET_{LST}, ET_{LST} based surface resistance (r_s), snow depth (SD), snow cover fraction based on Moderate Resolution Imaging Spectroradiometer (SCF_{MODIS}), air temperature (T_a), normalized difference vegetation index based on Advanced Very High Resolution Radiometer ($NDVI_{AVHRR}$), NDVI based on MODIS ($NDVI_{MODIS}$), leaf area index based on MODIS (LAI_{MODIS}), and LAI based on Copernicus Global Land Service (LAI_{CGLS}). Growing season represents the period from April to September and the seasons are represented by 3-months period labeled by the combination of the first letter of each month. The strength of the correlation is visualized by intensity of the color, where red depicts a negative whilst blue a positive correlation. The crosses indicate insignificant correlation ($p > 0.05$) and the circles indicate no data during the period. (For interpretation of the references to color in this figure legend, the reader is referred to the web version of this article.)

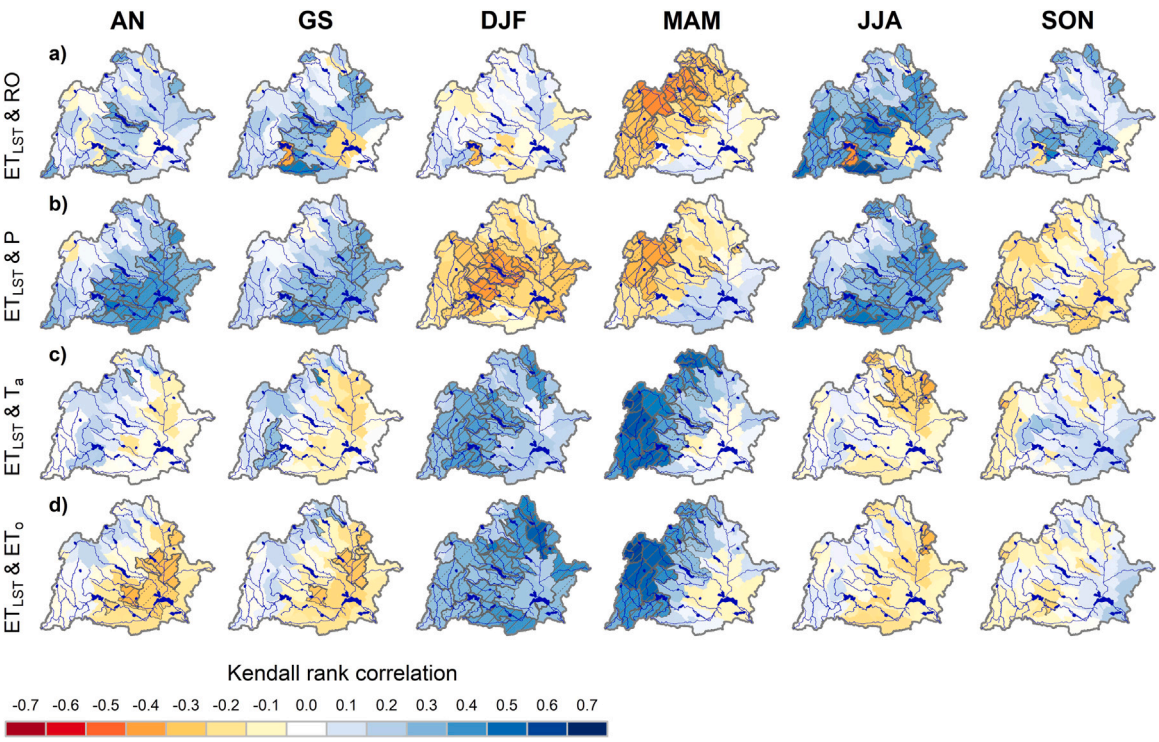

Fig. 9. Correlation of (a) land surface temperature based actual evapotranspiration (ET_{LST}) and runoff (RO), (b) ET_{LST} and precipitation (P), (c) ET_{LST} and air temperature (T_a), and (d) ET_{LST} and reference evapotranspiration (ET_o) for 2001–2020. The columns with plots represent different time scales: annual (AN), growing season (GS), i.e. April to September, and seasons, i.e. 3-months period labeled by the combination of the first letter of each month. The significant correlations ($p \leq 0.05$) are indicated by crosshatch lines while marginally significant correlations ($0.05 > p \leq 0.1$) by dotted lines.

3.3. Attribution of runoff trends

The partial derivatives of $RO = P - ET_{LST}$, where ET_{LST} is further decomposed by the partial derivatives of the Penman-Monteith model with varying r_s, were used to analyze the contributions of different drivers of RO for the period 2001–2020. At the annual time scale, the significant decline in RO in higher elevation areas was primarily driven by the decline in P (Fig. 10b) but also by increases in T_a (Fig. 10e) and decreases in RH (Fig. 10f), i.e. all negative contributions. A substantial positive contribution was also due to increases in r_s (Fig. 10h) which more or less compensated the negative contributions of T_a and RH leading to very small and insignificant changes in ET_{LST} (Fig. 10c). The magnitude of contributions by $R_n - G$ and u were in most cases negligible compared to the other drivers.

The spring months were characterized by the most pronounced decline in RO with significant negative trends over the major parts of the basin and especially all water source areas (Fig. 10a). The attribution analysis for the spring months again confirms the pivotal role of the decline in P (Fig. 10b) followed by decreases in RH (Fig. 10f) and increases in T_a (Fig. 10e) on the negative RO trends. During the spring months, r_s showed only small positive trends (Fig. 10h) with the result that the negative contribution of RH and T_a were not compensated, leading to a negative contribution of ET (Fig. 10c).

During the summer months, the decreasing trends in RO were significantly smaller as compared to the annual or spring values (Fig. 10a). The contributions to decreasing RO were again dominated by P (Fig. 10b), T_a (Fig. 10e) and RH (Fig. 10f). Since r_s showed strong positive trends, its positive contribution (Fig. 10h) compensated the negative contributions of T_a and RH leading to negative trends in ET (Fig. 10c) and its positive contribution to the water balance. It is interesting to note that while u showed negative trends over all time blocks, its contribution to the water balance was positive in spring months but negative during the summer months (Fig. 10g).

The contributions to the water balance for all analyzed time blocks and either for the entire basin, or the higher or lower elevation areas (threshold at 450 m a.s.l. based on Fig. 9), are summarized in Fig. 11. It should be remembered that the contributions to RO at sub-annual time scales must be treated with caution since, at these time scales, the varying storage term plays a significant role. This is very apparent in the comparison of changes in RO and contributions to these changes by P and ET_{LST} which are mostly in balance at the annual level (a perfect match cannot be achieved due to accumulation of various errors including the fact that the changes are inferred from the temporal trends) while they are generally negative in spring and the summer months. The positive balance is then observed in the fall months.

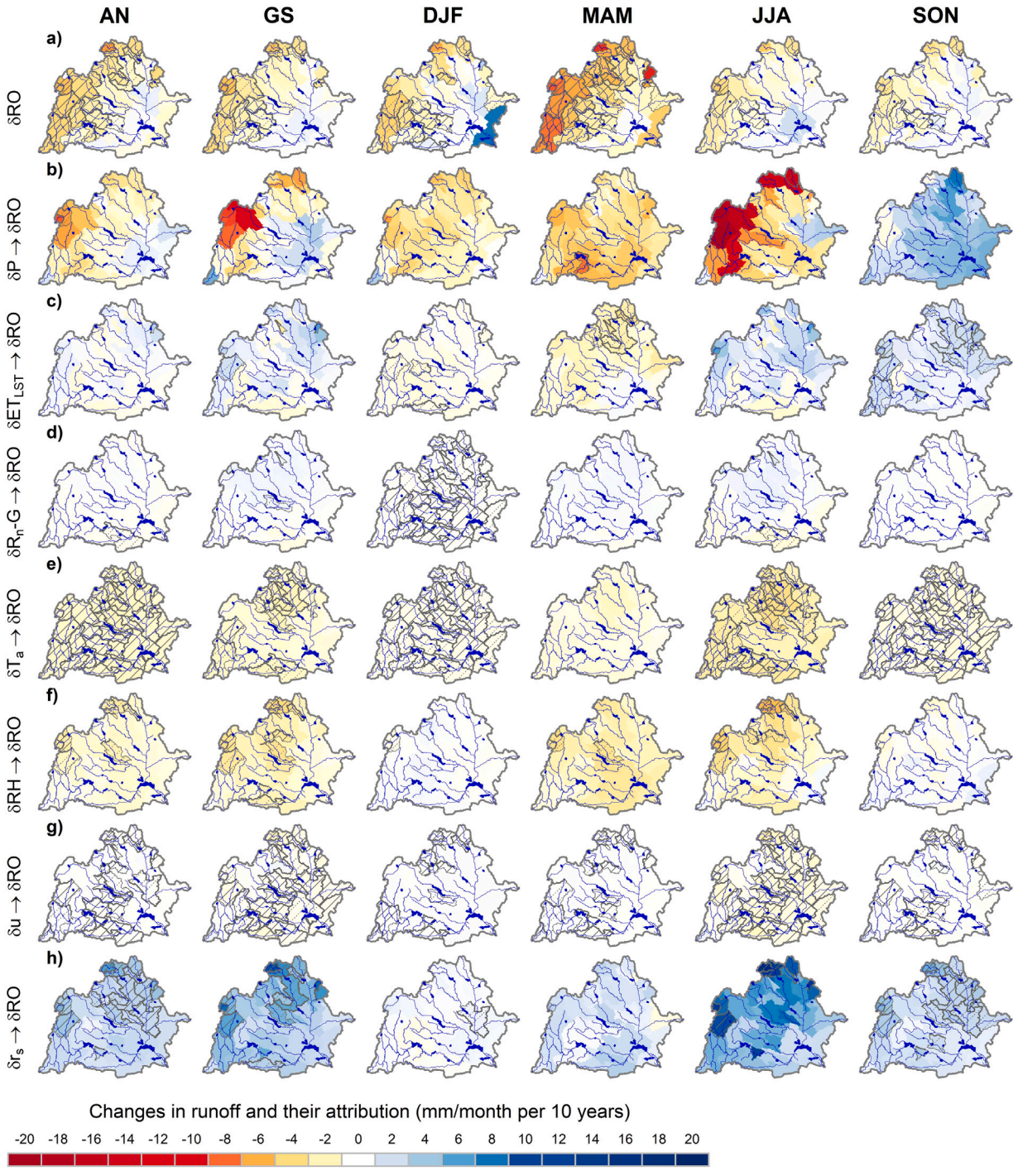

Fig. 10. (a) Changes in runoff (δRO) and (b–h) the contributions of changes in its drivers for the period 2001–2020. The arrow depicts the causal dependence of (δRO) on changes (δ) in its driver represented by (b) precipitation (P), (c) land surface temperature based actual evapotranspiration (ET_{LST}), (d) available energy being the difference between net radiation (R_n) and soil heat flux (G), (e) air temperature (T_a), (f) relative humidity (RH), (g) wind speed (u), and ET_{LST} based surface resistance (r_s). The columns with plots represent different time scales: annual (AN), growing season (GS), i.e. April to September, and seasons, i.e. 3-months period labeled by the combination of the first letter of each month. The significant trends ($p \leq 0.05$) are indicated by crosshatch lines while marginally significant trends ($0.05 > p \leq 0.1$) by dotted lines.

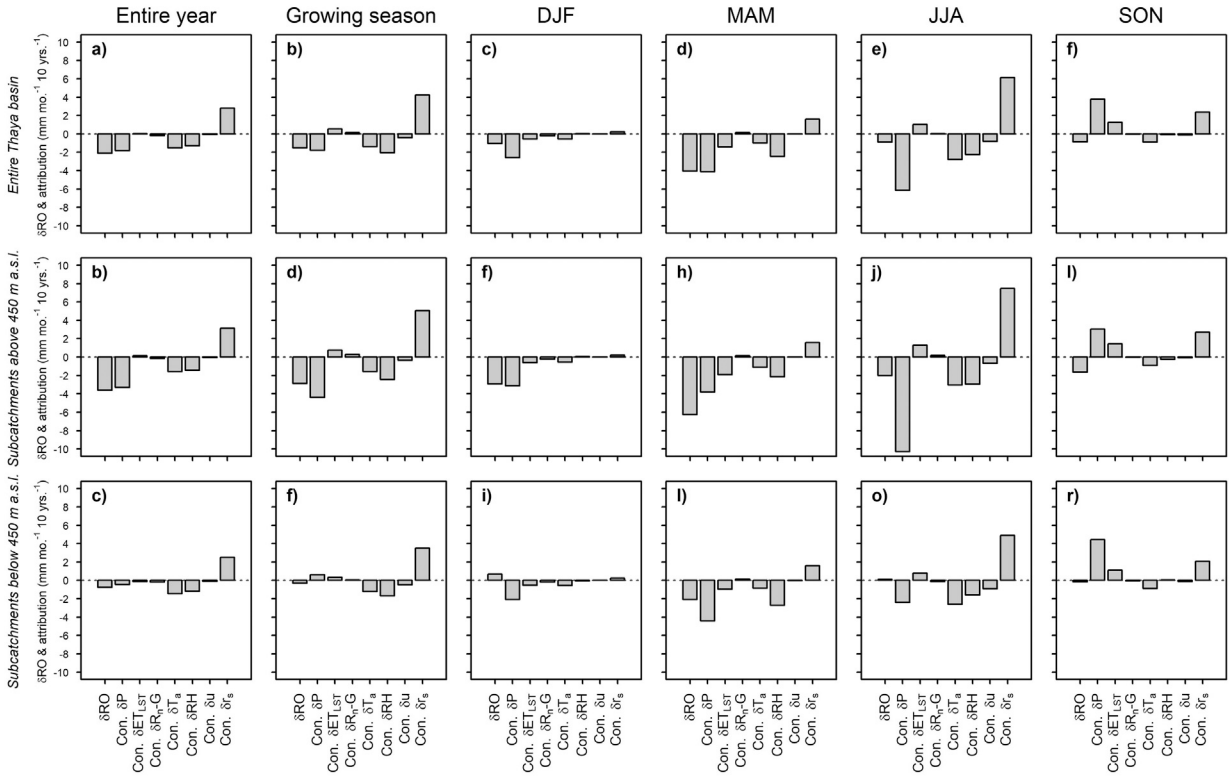

Fig. 11. Changes in runoff (δRO) and the contributions (Con.) of changes in its drivers for the period 2001–2020. The drivers are represented by precipitation (P), land surface based actual evapotranspiration (ET_{LST}), available energy being the difference between net radiation (R_n) and soil heat flux (G), air temperature (T_a), relative humidity (RH), wind speed (u), and ET_{LST} based surface resistance (r_s). The columns with plots represent different time scales where growing season stands for April to September, and seasons, i.e. 3-months periods, are labeled by the combination of the first letter of each month.

3.4. Evaporative vs. dryness index - Budyko analysis

By plotting ET_o/P *vs.* ET_{LST}/P, representing the aridity index and evaporative index, respectively, a Budyko (1974) diagram was obtained (Fig. 12). The long-term (2001–2020) mean of ET_o/P *vs.* ET_{LST}/P overestimated the theoretical Budyko (1974) curve (Fig. 12a). The fit of the parametric curve (Choudhúry, 1999) using the mean values weighted by the size of the subcatchment yielded a value of $n = 2.76$. The mean and median values are generally distributed more in the area with $ET_o/P > 1$ suggesting a rather arid climate and low RO in the majority of the subcatchments. The values representing the 25th percentile of the aridity index (and with them the paired evaporative index) were from 60% smaller than unity suggesting that under 5 years from the period 2001–2020 at each subcatchment (note that the years differ for different parts of basin and they were 2001, 2002, 2004, 2006, 2009, 2010, 2013, 2014 and 2020) ET of a larger number of subcatchments is limited by energy and not by water. When considering the minimum of the aridity index, nearly all subcatchments have a value smaller than unity suggesting that there are cases when nearly the entire basin is not limited by water (depending on the area it was 2001, 2002, 2010 or 2020). On the other hand, the values representing the 75th percentile of the aridity index where from 88% cases larger than unity suggesting that under 5 years (represented by 2003, 2008, 2011, 2012, 2015, 2016, 2017, 2018 and 2019) majority of the basin was limited by water. Finally, by considering the maximum of aridity index, all subcatchments have its value larger than unity indicating that entire basin was limited by water (depending on the area it was either the 2003, 2015, 2017 or 2018). Moreover, during the dry year $ET_{LST}/P > 1$ suggests a depletion of the overall storage by ET which is temporarily possible.

Analysis of the decadal trends in ET_o/P and ET_{LST}/P over the 2001–2020 allows us to visualize the shifts in the Budyko space (Fig. 12b). This analysis indicates that nearly the entire basin (except for two subcatchments with water reservoirs) is shifting along the trajectory of the Budyko curve to the right, i.e. increasing aridity and decreasing water RO/P and towards water limitation over the entire basin. The mean shift along the abscissa is 0.09 while the maximum is 0.18 per 10 years.

3.5. Overall water storage and climatic water deficits

At the annual time scale, $P - ET_{LST} - RO$ of the entire basin can be interpreted as the change of the overall storage term. Over the longer term, this change converges to zero while there are years with deficits (e.g. the already mentioned dry years 2003,

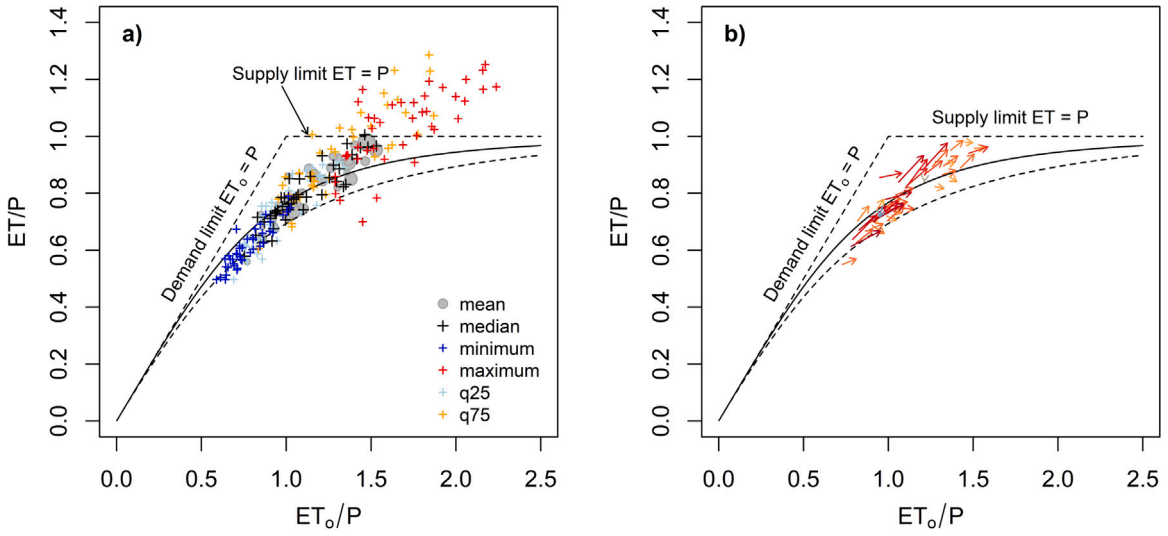

Fig. 12. (a) Budyko diagram with the aridity index (reference evapotranspiration ET_o divided by precipitation P) on the abscissa and evaporative index (land surface based actual evapotranspiration ET_{LST} divided by P) on the ordinate. The gray points represent the long-term (2001–2020) averages of these two indices for each subcatchment and the black line a fitted curve with weighting by the subcatchment size. For comparison, the dashed curve depicts the original Budyko relation. The crosses represent minimum, 25th, 50th (median), 75th percentiles and maximum of the aridity index for each subcatchment and with each aridity index associated evaporative index to show year-to-year variation within the Budyko space. (b) Budyko diagram with arrows representing the trends per decade where the colors go from light blue to dark blue if the tendency is towards decreasing aridity, and the colors go from light orange to dark red if the tendency is towards increasing aridity. (For interpretation of the references to color in this figure legend, the reader is referred to the web version of this article.)

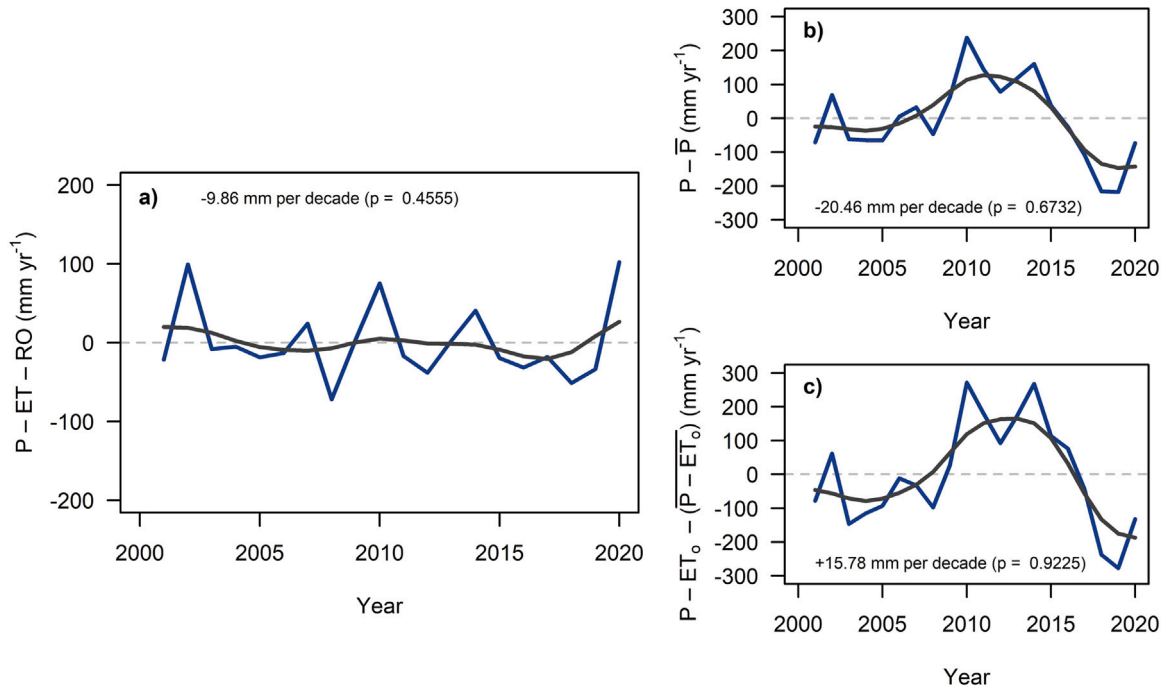

Fig. 13. (a) Cumulative overall water storage of the entire Thaya river basin calculated as the difference between precipitation (P), land surface temperature based actual evapotranspiration (ET_{LST}) and runoff (RO); (b) cumulative P anomaly; and (c) cumulative climatic water balance (P–ET_o) anomaly. The overbar denotes temporal average over the period 2001–2020.

2007, 2012, 2015–2019) and years with surplus (e.g. the wet years 2002, 2010 or 2020). When this change of the storage term is accumulated (Fig. 13a), one can verify if the whole system is in equilibrium (this should be the case at least for long time scales) or shows some trends (which can be real but may also point to systematic errors in any of the three variables). Fig. 13a suggests that the entire basin is in a water balance equilibrium with insignificant declining trends. Notable is the dry period 2015–2019

when the cumulative changes in the storage term showed the most persistent negative anomaly. Fig. 13a also suggests that without the wet years 2009 and in particular 2010, the trend of the overall storage would be more pronounced and the cumulative storage would likely reach more negative values. However, Fig. 13a also suggests relatively small amplitudes of the cumulative storage term. This is to be expected given that the wet years characterized by a large water surplus (such as 2002 and 2010) have significantly higher RO while the dry years, such as 2007 or the period 2015–2019, are characterized by significant reductions of ET precluding further basin desiccation. Such compensating mechanisms are not included in the standard climatological concept of accumulating anomalies of P (Fig. 13b) or $P - ET_o$ (Fig. 13c). These two terms both show much larger amplitudes. Worth mentioning is also the change between 2014 and 2018–2019 where in the case $P - ET_{LST} - RO$ the difference was 92 mm while in the case of P the difference was 379 mm and in the case of $P - ET_o$ it was 545 mm. Choice of these variables thus leads to significantly different interpretations of the basin deficit, although all have their own justification, since the climatological water deficit accurately highlights shifts in climatic conditions but does not express the amount of water needed for return to the normal conditions.

4. Discussion

This study aimed at understanding the temporal trends in a comprehensive set of hydroclimate and related variables in the Thaya river basin over the 1981–2020 period and in the case of some more recent remote sensing datasets, for the 2001–2020 period. Based on previous studies (Trnka et al., 2015, 2016; Brázdil et al., 2021; Zahradníček et al., 2021; Orság et al., 2022; Duethmann and Blöschl, 2018), we expected positive trends in T_a and ET_o yet no trends in P. In line with these trends, we hypothesized that positive trends in ET_o will lead also to positive trends in ET, at least in headwater catchments with higher elevation. We further conjectured that the increase in ET combined with stagnation of P will lead to a reduction of RO. In other words, we assumed that the water source areas of the basin are prevailingly limited by energy and that the positive trends in T_a and ET_o are an opportunity for ET to be increased. This increase of ET will have negative consequences for RO under the assumption of no trends in P. The results generally confirmed the already reported trends for T_a and ET_o and no trends in P; however, the original hypotheses were only partly confirmed since the expected mechanisms manifested themselves only in specific parts of the season.

Analysis at the annual time scale for the period 1981–2020 showed an insignificant increase in ET_{WB} and an insignificant decrease in RO. For the period 2001–2020, annual ET_{WB} showed a small insignificant increase while ET_{LST} decrease and annual RO over the entire basin showed statistically significant decrease of 24.80 mm yr^{-1} per decade. Note that the values of ET_{WB} at a sub-annual time scale must be treated with caution and may be indicative of changes in unaccounted storage terms, which preclude accurate determination of ET from P and RO measurements at such short time scales. The greatest contribution to these annual trends occurred due to a significant reduction of RO during the spring months. A significant spring RO reduction was detected for both periods - i.e.1981–2020 as well as 2001–2020. This reduction was associated with a significant decline of SD during the winter accompanied by earlier disappearance of snow and also increase of NDVI and LAI during the spring (caused by earlier start of the vegetation growth) and insignificant increase in ET_{LST}. Further, although the trends in P as well as $P - ET_o$ were insignificant at the annual and seasonal levels, they were both negative during the spring months and $P - ET_o$ showed the strongest reduction just during springs in the case of 1981–2020 with the strongest contribution by April. During the 2001–2020 this reduction was even more pronounced (with the strongest contribution by March closely followed by April) but was lower than the summer reduction $P - ET_o$. The warm and dry anomalies in Central Europe during the spring months were pointed out also by other authors (Brázdil et al., 2021; Hanel et al., 2018; Jaagus et al., 2022; Ionita et al., 2020; Zahradníček et al., 2021). As one of the main triggers of negative $P - ET_o$ anomaly is considered a multiyear recurrent high-pressure system centered over the North Sea and northern Germany and a decline in the temperature gradient between the Arctic region and the mid-latitudes diverting the moisture transport from the Atlantic northward (Ionita et al., 2020). A general increase in frequency of anticyclonic circulation types and decrease in frequency of some cyclonic types during spring in central Europe was also found by other authors (Brázdil et al., 2022b; Hofstätter et al., 2018). At the same time, the warmer spring with a higher amount of R_g and higher VPD (or lower RH) are the main precursors of higher ET_o and also ET which is often not limited by soil water availability in this early part of the year. It is worth mentioning that these were exactly the attributes of springs antecedent to the important drought events in 2003, 2007, 2012 and 2018. The mechanisms of drought propagation from spring to summer were extensively discussed e.g by Schär et al. (1999) or Miralles et al. (2019).

The correlation analysis applied in this study implies that the combination of warmer and drier springs is intensifying ET in the higher elevation parts of the Thaya river basin but has almost no or even negative effects on ET in lower elevation areas. This suggests that during the spring months, the higher elevation parts of the basin are limited by energy and that for these areas the warmer springs and earlier start of the growing season significantly enhance ET and likely also ecosystem productivity as evidenced by positive trends in LAI and NDVI in these areas and the correlations with LAI and NDVI. This is, however, not the case for the lower elevation areas during the spring and for the entire basin during the summer when the entire basin shows strong negative correlations of T_a with LAI and NDVI whereas a positive correlation of P with LAI and NDVI. This means that in summer, warmer and drier weather conditions are associated with increased drought stress. It is further evident that these correlations are much stronger during the period 2001–2020 than in the longer period 1981–2020, clearly providing an evidence of more arid climate conditions during the later period. The correlation of P and ET during the summer is also positive, however significant only in the lowlands, further demonstrating that ET in these parts of the basin is more limited by water availability. Note that the above-mentioned behavior is valid primarily for rain-fed areas and that alluvial areas with vegetation benefiting from access to the groundwater table in lowlands may act rather as the higher elevation areas - i.e. the warmer springs yet not limited by water may increase ET and productivity which can compensate the potential reduction due to summer droughts (Kowalska et al., 2020).

In order to disentangle the main drivers of these changes, an attribution analysis was performed. This analysis was based on partial derivatives of RO ≈ $P - ET_{LST}$ (Betts et al., 2007) and the decomposition of ET_{LST} following Beven (1979). Although the decomposition of ET can be approximated by Taylor-series expansion of higher orders, we found that the first order is sufficiently accurate, at least for the purpose of the attribution analysis. At the annual time scale, the contribution to negative trends in RO of the entire Thaya river basin during the period 2001–2020 was mainly caused by the negative tendency in P followed by significant trends in T_a and RH. The contribution of these variables to negative trends in RO was partly compensated by positive trends in r_s. A small contribution to negative RO was also caused by increasing tendencies in R_g driving $R_n - G$. Interestingly, the significantly decreasing trend in u contributed also (although very negligibly) to negative trends in RO at an annual time scale and to a larger extent during the summer period. Although it may appear as counterintuitive since one may conjecture that lower u will translate into lower ET, the opposite may be the case. Monteith (1965) already described the complex role of u in ET and introduced so-called critical value of r_s below which an increase of u will cause an increase of ET, yet above which an increase of u will cause a decrease of ET. In other words, the critical value of r_s determines whether the higher u will mean an increase of the atmospheric evaporative demand (i.e. values below the critical value) or rather increase of cooling due transport of fresh air into the boundary layer warmed by the surface with rather high Bowen ratio (i.e. values above the critical value). Since ET_o represents a hypothetical reference grass with no water limitation and has prescribed r_s of 70 s m^{-1} (Allen et al., 1998), the decreasing trends in u over the Thaya river basin almost always contributed to the decreasing trends in ET_o (McVicar et al., 2012). However, in the case of observed ET_{LST} for the Thaya river basin, r_s was often higher than its critical value and hence caused the negative trends in u do contribute to the increase of ET due to lack of cooling and consequently to a decrease in RO. This phenomenon is most pronounced in dry and warm summer months. Such a bidirectional role of u should be taken into account when adaptation measures aiming to reduce ET by increasing landscape aerodynamic roughness are considered. This identified significant negative trend of u is a subject of ongoing discussion not only in the regional (Zahradníček et al., 2019) but also global context (McVicar et al., 2012). The main causes of these negative trends are, among others, often explained by increasing land surface roughness, instrumental issues but also mesoscale circulation changes (McVicar et al., 2012). These trends in u likely caused relatively small increases in ET_o as compared to the pronounced and consistent trends in T_a. Another important feature of the attribution analysis is a contribution of increasing RH on increase of ET and decrease of RO. By its extent, the contribution of RH is similar to the contribution of T_a. The role of RH (or VPD) is relevant from the perspective of potential evaporation and the fact that numerous hydrological models are relying on potential evaporation which is not accounting for the role of air humidity (e.g. Oudin et al. 2005). Although RH (or VPD) is not independent of T_a, care should be taken when largely different conditions are simulated (e.g. future climate projections). The study by Duethmann and Blöschl (2018) reported an increasing ET_{WB} in a number of catchments in Austria over the period 1977–2014 driven mainly by increasing R_g, T_a and lengthening of the active growing season (positive trend in NDVI). In our study, increasing ET_{WB} and NDVI in 1981–2020 was also observed, with some flattening during the last two decades. For the period of 2001–2020 when the ET_{LST} was available, no trend in ET was observed and this was mainly caused by water limitations. Both of the studies (Duethmann and Blöschl, 2018, and this study) indicate a hiatus in ET increasing in Central Europe during the first two decades of the 21st century driven either by increasing T_a and ET_o, or increasing T_a and ET_o together with decreasing P. Our study further shows that these changes have significant impacts on RO in the Thaya river basin and possibly also other Central European river basins with similar aridity index.

This study introduces a regionally unique 20-year long dataset of the remotely sensed ET based on the ALEXI model to study the hydrology at the level of the entire basin and individual subcatchments. Previous studies from this Central European region used ALEXI-based ET only to a limited extent with the main focus on crop yields prediction and drought impacts evaluation (Anderson et al., 2016; Crocetti et al., 2020; Jurečka et al., 2021; Bartošová et al., 2022). Given the good water balance closure of $P \approx RO+ET_{LST}$ presented above, this study supports its validity for the water balance studies and unlocks new opportunities for further utilization within hydrological modeling efforts where it can provide an important constraint in the calibration/validation process (Mendiguren et al., 2017; Demirel et al., 2018) but also more detailed insights into studying droughts (Crocetti et al., 2020). Besides the hydrology, the ALEXI-based ET can also be useful for addressing large scale processes related to precipitation recycling or water vapor mass and heat conservation of a given area within the so-called complementary hypothesis (Bouchet, 1963; Brutsaert and Parlange, 1998). This hypothesis suggests that at large scales, the sum of ET_o and ET is conserved for a fixed available energy level over time since an increase in ET should cause a decrease in ET_o and *vice versa*. In the Thaya river basin, the computed coefficients of variation of annual ET_{LST}, ET_o and $ET_o + ET_{LST}$ were 4.7%, 6.0% and 3.7%, respectively, indicating a certain amount of complementary mechanisms to be valid even at the scale of this basin. These mechanisms must be taken into account when adaptation measures aiming to modulate landscape ET are considered. As such, hypothetically, efforts in reducing ET by crops with lower water requirements may cause higher ET_o and hence lead to an originally unintended increase of ET. At the same time, non-convergence of $ET_o + ET$ to a constant value indicates that the basin extent is far too limited to allow ignoring advection of moisture and heat and to expect a significant regional P recycling ratio (i.e. the ratio of regionally recycled P to total P in a region). In fact, according to van der Ent et al. (2010), the regional P recycling ratio in the region of the Thaya river basin is about ~1%. Further, the continental P recycling ratio of this region is about ~40% meaning that this amount of P origins from land while the remaining ~60% origins from the sea and the ocean (van der Ent et al., 2010). Finally, the global study by van der Ent and Savenije (2011) suggests that the water evaporated from the Czech territory is likely recycled to P some 3 000 km eastwards. These findings must be taken into account when hypothetical adaptation measures strive to alter regional ET, e.g. through land-use change.

The hydroclimate trends described in this study mirror also in notable shifts towards an increasing aridity (ET_o/P), increased ET/P and decreased P/RO within the Budyko space. The resulting parameter $n = 2.76$ describing the shape of the Budyko curve exceeds the original Budyko predictions and ranks among the highest ones reported by Choudhúry (1999) and Li et al. (2013). The

higher values might be partly explained by different choice of the potential ET formulation but in general, they are suggesting an important role of vegetation in P partitioning within the Thaya river basin. Nevertheless, since fitting of this parameter on the values of ET/P and ET_o/P along their trends led only to a minor increase of n, we conjecture that the observed positive trends in vegetation variables (NDVI and LAI) play much less prominent role on P partitioning than the changes of climatic variables. This study provides evidence about the trends during the last 40 years characterized mainly by increasing T_a and ET_o while stagnating P leading to regional water deficit. The climate projections generally support that this direction towards aridity in the summer half-year will be progressively worsening throughout the 21st century with different intensities conditioned by unknown socioeconomic pathways and emission scenarios as well by uncertainties in climate models (Hari et al., 2020; Oulehle et al., 2021; Trnka et al., 2022b). As shown, the real hydrological deficits are smaller than those inferred from the climatological analysis due to several self-compensating processes (e.g. the low soil moisture limited ET preventing extreme soil water deficits); however, it must be taken into account that the long-lasting deficit periods affect not only hydrology but also ecosystem productivity, biodiversity, and ultimately the landscape carbon balance.

5. Conclusions

This study combined terrestrial and remote sensing data to provide new insights into the complex interplay of climate, vegetation, and the hydrological cycle of the Thaya river basin in Central Europe. The overall trends were characterized by significantly increasing T_a and ET_o, along with statistically non-significant trends in P and significant decreases of RO. The negative trends in RO were attributed to non-significant decreases in P and RH and significant increases of T_a, suggesting that even statistically non-significant trends should be of interest, since complex response variables such as ET and RO are dependent on several drivers whose effects may accumulate or further interact. The identified positive trends in vegetation indices (represented by NDVI and LAI) were shown to be important features of the hydrological system, potentially meaning higher vegetation water requirements; however, these trends have flattened during the last decade characterized by more pronounced drought stress and water limitations. ET in the higher elevation parts of the basin is mainly limited by energy while in the lower parts by available water. Nevertheless, this feature is relevant only during the spring whereas during the summer months, ET in the entire basin is often limited by water. The results of this study suggest that complex adaptation to climate change will be needed to sustain the water dependent sectors operating in the Thaya river basin characterized by an increasing aridity. These measures must reflect the different hydroclimate relationships across the altitudinal gradient characterized by water and energy limits that are shifting over time, as well as several local, regional up to continental scale (self-)compensating mechanisms discussed in this study.

CRediT authorship contribution statement

Milan Fischer: Conceptualization, Methodology, Formal analysis, Investigation, Writing – original draft, Writing – review & editing. **Petr Pavlík:** Methodology, Formal analysis, Investigation, Writing – original draft, Writing – review & editing. **Adam Vizina:** Conceptualization, Methodology, Writing – original draft, Funding acquisition. **Jana Bernsteinová:** Methodology, Investigation, Writing – original draft. **Juraj Parajka:** Resources, Methodology, Writing – original draft. **Martha Anderson:** Resources, Methodology, Writing – original draft. **Jan Řehoř:** Methodology, Writing – original draft. **Jana Ivančicová:** Resources, Data curation, Writing – original draft. **Petr Štěpánek:** Data curation, Methodology, Writing – original draft. **Jan Balek:** Data curation, Methodology. **Christopher Hain:** Resources, Data curation, Methodology. **Pavel Tachecí:** Conceptualization, Methodology, Investigation. **Martin Hanel:** Resources, Data curation, Writing – original draft. **Petr Lukeš:** Resources, Data curation, Writing – original draft. **Monika Bláhová:** Resources, Data curation, Writing – original draft. **Jiří Dlabal:** Resources, Data curation. **Pavel Zahradníček:** Formal analysis, Writing – original draft. **Petr Máca:** Conceptualization, Writing – original draft. **Jürgen Komma:** Resources, Writing – review & editing. **Nad'a Rapantová:** Methodology, Writing – original draft. **Song Feng:** Conceptualization, Methodology, Writing – original draft. **Petr Janál:** Resources, Data curation. **Evžen Zeman:** Project administration, Writing – original draft. **Zdeněk Žalud:** Project administration, Funding acquisition. **Günter Blöschl:** Methodology, Writing – original draft, Funding acquisition. **Miroslav Trnka:** Conceptualization, Supervision, Funding acquisition, Writing – original draft.

Declaration of competing interest

The authors declare that they have no known competing financial interests or personal relationships that could have appeared to influence the work reported in this paper.

Data availability

Data will be made available on request.

References

Alfieri, L., Feyen, L., Dottori, F., Bianchi, A., 2015. Ensemble flood risk assessment in Europe under high end climate scenarios. Global Environ. Change 35 (1), 199–212.

Allen, R.G., Pereira, L.S., Raes, D., Smith, M., 1998. Crop Evapotranspiration: Guidelines for Computing Crop Water Requirements. Irrigation and Drainage Paper No. 56, FAO, Rome, Italy.

Anderson, M.C., Hain, C.R., Jurecka, F., Trnka, M., Hlavinka, P., Dulaney, W., Otkin, J.A., Johnson, D., Gao, F., 2016. Relationships between the evaporative stress index and winter wheat and spring barley yield anomalies in the Czech Republic. Clim. Res. 70 (2–3), 215–230.

Anderson, M., Norman, J., Diak, G., Kustas, W., Mecikalski, J., 1997. A two-source time-integrated model for estimating surface fluxes using thermal infrared remote sensing. Remote Sens. Environ. 60 (2), 195–216.

Anderson, M.C., Norman, J.M., Mecikalski, J.R., Otkin, J.A., Kustas, W.P., 2007. A climatological study of evapotranspiration and moisture stress across the continental United States based on thermal remote sensing: 1. Model formulation. J. Geophys. Res.: Atmos. 112 (D10).

Bartošová, L., Fischer, M., Balek, J., Bláhová, M., Kudláčková, L., Chuchma, F., Hlavinka, P., Možný, M., Zahradníček, P., Wall, N., Hayes, M., Hain, C., Anderson, M., Wagner, W., Žalud, Z., Trnka, M., 2022. Validity and reliability of drought reporters in estimating soil water content and drought impacts in central Europe. Agricult. Forest Meteorol. 315, 108808.

Betts, R.A., Boucher, O., Collins, M., Cox, P.M., Falloon, P.D., Gedney, N., Hemming, D.L., Huntingford, C., Jones, C.D., Sexton, D.M.H., Webb, M.J., 2007. Projected increase in continental runoff due to plant responses to increasing carbon dioxide. Nature 448 (7157), 1037–1041.

Beven, K., 1979. A sensitivity analysis of the Penman-Monteith actual evapotranspiration estimates. J. Hydrol. 44 (3), 169–190.

Blahušiaková, A., Matoušková, M., Jenicek, M., Ledvinka, O., Kliment, Z., Podolinská, J., Snopková, Z., 2020. Snow and climate trends and their impact on seasonal runoff and hydrological drought types in selected mountain catchments in Central Europe. Hydrol. Sci. J. 65 (12), 2083–2096.

Blöschl, G., Hall, J., Parajka, J., Perdigão, R., Merz, B., Arheimer, B., Aronica, G., Bilibashi, A., Bonacci, O., Borga, M., Čanjevac, I., Castellarin, A., Chirico, G., Claps, P., Fiala, K., Frolova, N., Gorbachova, L., Gül, A., Hannaford, J., Harrigan, S., Kireeva, M., Kiss, A., Kjeldsen, T., Kohnová, S., Koskela, J., Ledvinka, O., Macdonald, N., Mavrova-Guirguinova, M., Mediero, L., Merz, R., Molnar, P., Montanari, A., Murphy, C., Osuch, M., Ovcharuk, V., Radevski, I., Rogger, M., Salinas, J., Sauquet, E., Šraj, M., Szolgay, J., Viglione, A., Volpi, E., Wilson, D., Zaimi, K., 2017. Changing climate shifts timing of European floods. Science 357 (6351), 588–590.

Bouchet, R., 1963. Evapotranspiration reelle at potentielle, signification climatique. Int. Assoc. Hydrol. Sci. 62, 134–142.

Brázdil, R., Zahradník, P., Szabó, P., Chromá, K., Dobrovolný, P., Dolák, L., Trnka, M., Řehoř, J., Suchánková, S., 2022a. Meteorological and climatological triggers of notable past and present bark beetle outbreaks in the Czech Republic. Clim. Past 18 (9), 2155–2180.

Brázdil, R., Zahradníček, P., Dobrovolný, P., Řehoř, J., Trnka, M., Lhotka, O., Štěpánek, P., 2022b. Circulation and climate variability in the Czech Republic between 1961 and 2020: A comparison of changes for two "normal" periods. Atmosphere 13 (1).

Brázdil, R., Zahradníček, P., Dobrovolný, P., Štěpánek, P., Trnka, M., 2021. Observed changes in precipitation during recent warming: The Czech Republic, 1961–2019. Int. J. Climatol. 41 (7), 3881–3902.

Brutsaert, W., Parlange, M.B., 1998. Hydrologic cycle explains the evaporation paradox. Nature 396 (6706), 30.

Budyko, M., Budyko, M., Miller, D., 1974. Climate and Life. In: International Geophysics Series, Academic Press.

Chen, C., Wang, L., Myneni, R.B., Li, D., 2020. Attribution of land-use/land-cover change induced surface temperature anomaly: How accurate is the first-order taylor series expansion? J. Geophys. Res. Biogeosci. 125 (9), e2020JG005787.

Choudhúry, B.J., 1999. Evaluation of an empirical equation for annual evaporation using field observations and results from a biophysical model. J. Hydrol. 216 (1), 99–110.

Crocetti, L., Forkel, M., Fischer, M., Jurečka, F., Grlj, A., Salentinig, A., Trnka, M., Anderson, M., Ng, W.-T., Kokalj, Ž., Bucur, A., Dorigo, W., 2020. Earth Observation for agricultural drought monitoring in the Pannonian Basin (Southeastern Europe): current state and future directions. Reg. Environ. Change 20 (4), 123, Number: 4.

Demirel, M.C., Mai, J., Mendiguren, G., Koch, J., Samaniego, L., Stisen, S., 2018. Combining satellite data and appropriate objective functions for improved spatial pattern performance of a distributed hydrologic model. Hydrol. Earth Syst. Sci. 22 (2), 1299–1315.

Duethmann, D., Blöschl, G., 2018. Why has catchment evaporation increased in the past 40 years? A data-based study in Austria. Hydrol. Earth Syst. Sci. 22 (10), 5143–5158.

Feng, S., Fu, Q., 2013. Expansion of global drylands under a warming climate. Atmos. Chem. Phys. 13 (19), 10081–10094.

Fiala, T., Ouarda, T.B., Hladný, J., 2010. Evolution of low flows in the Czech Republic. J. Hydrol. 393 (3), 206–218.

Gao, F., Anderson, M., Daughtry, C., Karnieli, A., Hively, D., Kustas, W., 2020. A within-season approach for detecting early growth stages in corn and soybean using high temporal and spatial resolution imagery. Remote Sens. Environ. 242, 111752.

Hain, C.R., Anderson, M.C., 2017. Estimating morning change in land surface temperature from MODIS day/night observations: Applications for surface energy balance modeling. Geophys. Res. Lett. 44 (19), 9723–9733.

Hall, D.K., Riggs, G.A., 2011. Normalized-difference snow index (NDSI). In: Singh, V.P., Singh, P., Haritashya, U.K. (Eds.), Encyclopedia of Snow, Ice and Glaciers. Springer Netherlands, Dordrecht, pp. 779–780.

Hall, D.K., Riggs., G.A., 2021. MODIS/Terra Snow Cover Daily L3 Global 500 m SIN Grid, Version 61. NASA National Snow and Ice Data Center Distributed Active Archive Center, URL https://nsidc.org/data/MOD10A1/versions/61.

Hanel, M., Rakovec, O., Markonis, Y., Máca, P., Samaniego, L., Kyselý, J., Kumar, R., 2018. Revisiting the recent European droughts from a long-term perspective. Sci. Rep. 8 (1), 9499.

Hanel, M., Vizina, A., Máca, P., Pavlásek, J., 2012. A multi-model assessment of climate change impact on hydrological regime in the Czech Republic. J. Hydrol. Hydromech. 60 (3), 152–161.

Hari, V., Rakovec, O., Markonis, Y., Hanel, M., Kumar, R., 2020. Increased future occurrences of the exceptional 2018–2019 Central European drought under global warming. Sci. Rep. 10 (1), 12207.

Hlásny, T., Mátyás, C., Seidl, R., Kulla, L., Merganicová, K., 2014. Climate change increases the drought risk in Central European forests: what are the otions for adaptation? Forestry J. 60, 5–18.

Hofstätter, M., Lexer, A., Homann, M., Blöschl, G., 2018. Large-scale heavy precipitation over central Europe and the role of atmospheric cyclone track types. Int. J. Climatol. 38, e497–e517.

Ionita, M., Nagavciuc, V., Kumar, R., Rakovec, O., 2020. On the curious case of the recent decade, mid-spring precipitation deficit in central Europe. Npj Clim. Atmos. Sci. 3 (1), 49.

Jaagus, J., Aasa, A., Aniskevich, S., Boincean, B., Bojariu, R., Briede, A., Danilovich, I., Castro, F.D., Dumitrescu, A., Labuda, M., Labudová, L., Löhmus, K., Melnik, V., Möisja, K., Pongracz, R., Potopová, V., Řezníčková, L., Rimkus, E., Semenova, I., Stonevičius, E., Štěpánek, P., Trnka, M., Vicente-Serrano, S.M., Wibig, J., Zahradníček, P., 2022. Long-term changes in drought indices in eastern and central Europe. Int. J. Climatol. 42 (1), 225–249.

Jurečka, F., Fischer, M., Hlavinka, P., Balek, J., Semerádová, D., Bláhová, M., Anderson, M.C., Hain, C., Žalud, Z., Trnka, M., 2021. Potential of water balance and remote sensing-based evapotranspiration models to predict yields of spring barley and winter wheat in the Czech Republic. Agricult. Water Manag. 256, 107064.

Katul, G.G., Oren, R., Manzoni, S., Higgins, C., Parlange, M.B., 2012. Evapotranspiration: A process driving mass transport and energy exchange in the soil-plant-atmosphere-climate system. Rev. Geophys. 50 (3).
Kendall, M.G., 1938. A new measure of rank correlation. Biometrika 30 (1–2), 81–93.
Kendall, M., Gibbons, J.D., 1990. Rank Correlation Methods, fifth ed. A Charles Griffin Title.
Kliment, Z., Matouskova, M., Ledvinka, O., Královec, V., 2011. Trend analysis of rainfall-runoff regimes in selected headwater areas of the Czech Republic. J. Hydrol. Hydromech. 59 (1), 36.
Kowalska, N., Šigut, L., Stojanović, M., Fischer, M., Kyselová, I., Pavelka, M., 2020. Analysis of floodplain forest sensitivity to drought. Philos. Trans. R. Soc. B 375 (1810), 20190518.
Langhammer, J., Bernsteinová, J., 2020. Which aspects of hydrological regime in mid-latitude montane basins are affected by climate change? Water 12 (8).
Ledvinka, O., 2015. Evolution of low flows in Czechia revisited. Proc. Int. Assoc. Hydrol. Sci. 369, 87–95.
Li, D., Pan, M., Cong, Z., Zhang, L., Wood, E., 2013. Vegetation control on water and energy balance within the Budyko framework. Water Resour. Res. 49 (2), 969–976.
Liepert, B.G., Previdi, M., 2009. Do models and observations disagree on the rainfall response to global warming? J. Clim. 22 (11), 3156–3166.
Mann, H.B., 1945. Nonparametric tests against trend. Econometrica 13 (3), 245–259.
McVicar, T.R., Roderick, M.L., Donohue, R.J., Li, L.T., Niel, T.G.V., Thomas, A., Grieser, J., Jhajharia, D., Himri, Y., Mahowald, N.M., Mescherskaya, A.V., Kruger, A.C., Rehman, S., Dinpashoh, Y., 2012. Global review and synthesis of trends in observed terrestrial near-surface wind speeds: Implications for evaporation. J. Hydrol. 416–417, 182–205.
Mecikalski, J.R., Diak, G.R., Anderson, M.C., Norman, J.M., 1999. Estimating fluxes on continental scales using remotely sensed data in an atmospheric–land exchange model. J. Appl. Meteorol. 38 (9), 1352–1369.
Mendiguren, G., Koch, J., Stisen, S., 2017. Spatial pattern evaluation of a calibrated national hydrological model – a remote-sensing-based diagnostic approach. Hydrol. Earth Syst. Sci. 21 (12), 5987–6005.
Miralles, D.G., Gentine, P., Seneviratne, S.I., Teuling, A.J., 2019. Land–atmospheric feedbacks during droughts and heatwaves: state of the science and current challenges. Ann. New York Acad. Sci. 1436, 19–35.
Monteith, J.L., 1965. Evaporation and environment. In: Symposia of the Society for Experimental Biology. Vol. 19. pp. 205–234.
Mostowik, K., Siwek, J., Kisiel, M., Kowalik, K., Krzysik, M., Plenzler, J., Rzonca, B., 2019. Runoff trends in a changing climate in the Eastern Carpathians (Bieszczady Mountains, Poland). Catena 182, 104174.
Norman, J.M., Kustas, W.P., Humes, K.S., 1995. Source approach for estimating soil and vegetation energy fluxes in observations of directional radiometric surface temperature. Agricult. Forest Meteorol. 77, 263–293.
Orság, M., Fischer, M., Trnka, M., Brotan, J., Pozníková, G., Žalud, Z., 2022. Trends in air temperature and precipitation in southeastern Czech Republic, 1961–2020. Acta Univ Agric Et Silviculturae Mendelianae Brunensis 12.
Oudin, L., Hervieu, F., Michel, C., Perrin, C., Andréassian, V., Anctil, F., Loumagne, C., 2005. Which potential evapotranspiration input for a lumped Rainfall–Runoff model?: Part 2—Towards a simple and efficient potential evapotranspiration model for Rainfall–Runoff modelling. J. Hydrol. 303 (1), 290–306.
Oulehle, F., Fischer, M., Hruška, J., Chuman, T., Krám, P., Navrátil, T., Tesař, M., Trnka, M., 2021. The GEOMON network of Czech catchments provides long-term insights into altered forest biogeochemistry: From acid atmospheric deposition to climate change. Hydrol. Process. 35 (5), e14204.
Řehoř, J., Brázdil, R., Lhotka, O., Trnka, M., Balek, J., Štěpánek, P., Zahradníček, P., 2021. Precipitation in the Czech Republic in light of subjective and objective classifications of circulation types. Atmosphere 12 (11).
Schär, C., Lüthi, D., Beyerle, U., Heise, E., 1999. The soil–precipitation feedback: A process study with a regional climate model. J. Clim. 12.
Sen, P.K., 1968. Estimates of the regression coefficient based on Kendall's Tau. J. Amer. Statist. Assoc. 63 (324), 1379–1389.
Squintu, A.A., van der Schrier, G., Štěpánek, P., Zahradníček, P., Tank, A.K., 2020. Comparison of homogenization methods for daily temperature series against an observation-based benchmark dataset. Theor. Appl. Climatol. 140 (1), 285–301.
Štěpánek, P., Zahradníček, P., Farda, A., 2013. Experiences with data quality control and homogenization of daily records of various meteorological elements in the Czech Republic in the period 1961–2010. Időjárás 117 (1), 123–141.
Štěpánek, P., Zahradníček, P., Farda, A., Skalák, P., Trnka, M., Meitner, J., Rajdl, K., 2016. Projection of drought-inducing climate conditions in the Czech Republic according to Euro-CORDEX models. Clim. Res. 70, 179–193.
Štěpánek, P., Zahradníček, P., Huth, R., 2011. Interpolation techniques used for data quality control and calculation of technical series: an example of Central European daily time series. Időjárás 115 (1–2), 87–98.
Teuling, A., de Badts, E., Jansen, F., Fuchs, R., Buitink, J., Hoek van Dijke, A., Sterling, S., 2019. Climate change, reforestation/afforestation, and urbanization impacts on evapotranspiration and streamflow in Europe. Hydrol. Earth Syst. Sci. 23 (9), 3631–3652.
Theil, H., 1950. A rank-invariant method of linear and polynomial regression analysis, 1-2; confidence regions for the parameters of linear regression equations in two, three and more variables. Indag. Math. (N.S.) 1 (2).
Tong, R., Parajka, J., Komma, J., Blöschl, G., 2020. Mapping snow cover from daily Collection 6 MODIS products over Austria. J. Hydrol. 590, 125548.
Trnka, M., Balek, J., Štěpánek, P., Zahradníček, P., Možný, M., Eitzinger, J., Žalud, Z., H., F., M., T., P., N., Semerádová, D., Hlavinka, P., Brázdil, R., 2016. Drought trends over part of Central Europe between 1961 and 2014. Clim. Res. 70, 143–160.
Trnka, M., Bartošová, L., Grammatikopoulou, I., Havlík, P., Olesen, J.E., Hlavinka, P., Marek, M.V., Vačkářová, D., Skjelvåg, A., Žalud, Z., 2022a. The possibility of consensus regarding climate change adaptation policies in agriculture and forestry among stakeholder groups in the Czech Republic. Environ. Manag. 69 (1), 128–139.
Trnka, M., Brázdil, R., Balek, J., Semerádová, D., Hlavinka, P., Možný, M., Štěpánek, P., Dobrovolný, P., Zahradníček, P., Dubrovský, M., Eitzinger, J., Fuchs, B., Svoboda, M., Hayes, M., Žalud, Z., 2015. Drivers of soil drying in the Czech Republic between 1961 and 2012. Int. J. Climatol. 35 (9), 2664–2675.
Trnka, M., Kocmánková, E., Balek, J., Eitzinger, J., Ruget, F., Formayer, H., Hlavinka, P., Schaumberger, A., Horáková, V., Možný, M., Žalud, Z., 2010. Simple snow cover model for agrometeorological applications. Agricult. Forest Meteorol. 150 (7), 1115–1127.
Trnka, M., Vizina, A., Hanel, M., Balek, J., Fischer, M., Hlavinka, P., Semerádová, D., Štěpánek, P., Zahradníček, P., Skalák, P., Eitzinger, J., Dubrovský, M., Máca, P., Bělínová, M., Zeman, E., Brázdil, R., 2022b. Increasing available water capacity as a factor for increasing drought resilience or potential conflict over water resources under present and future climate conditions. Agric. Water Manag. 264, 107460.
Tureček, K., 2002. Methodological Instruction of the Ministry of Agriculture of the Czech Republic for the Preparation of the Water Management Balance of the River Basin. Ministry of Agriculture of the Czech Republic.
van der Ent, R.J., Savenije, H.H.G., 2011. Length and time scales of atmospheric moisture recycling. Atmos. Chem. Phys. 11 (5), 1853–1863.
van der Ent, R.J., Savenije, H.H.G., Schaefli, B., Steele-Dunne, S.C., 2010. Origin and fate of atmospheric moisture over continents. Water Resour. Res. 46 (9).
Vargas Godoy, M.R., Markonis, Y., Hanel, M., Kyselý, J., Papalexiou, S.M., 2021. The global water cycle budget: A chronological review. Surv. Geophys. 42 (5), 1075–1107.
Vormoor, K., Lawrence, D., Heistermann, M., Bronstert, A., 2015. Climate change impacts on the seasonality and generation processes of floods – projections and uncertainties for catchments with mixed snowmelt/rainfall regimes. Hydrol. Earth Syst. Sci. 19 (2), 913–931.
Wentz, F.J., Ricciardulli, L., Hilburn, K., Mears, C., 2007. How much more rain will global warming bring? Science 317 (5835), 233–235.
Yang, Y., Anderson, M.C., Gao, F., Hain, C.R., Semmens, K.A., Kustas, W.P., Noormets, A., Wynne, R.H., Thomas, V.A., Sun, G., 2017. Daily Landsat-scale evapotranspiration estimation over a forested landscape in North Carolina, USA, using multi-satellite data fusion. Hydrol. Earth Syst. Sci. 21, 1017–1037.
Zahradníček, P., Brázdil, R., Štěpánek, P., Řezníčková, L., 2019. Differences in wind speeds according to measured and homogenized series in the Czech Republic, 1961–2015. Int. J. Climatol. 39 (1), 235–250.
Zahradníček, P., Brázdil, R., Štěpánek, P., Trnka, M., 2021. Reflections of global warming in trends of temperature characteristics in the Czech Republic, 1961–2019. Int. J. Climatol. 41 (2), 1211–1229.